Journal of proteome research

Article

pubs.acs.org/jpr

The Liver Connexin32 Interactome Is a Novel Plasma Membrane-Mitochondrial Signaling Nexus

Stephanie L. Fowler,[†,‡] Mark Akins,[†,‡] Hu Zhou,[‡,§] Daniel Figeys,[*,‡] and Steffany A.L. Bennett[*,†,‡]

[†]Neural Regeneration Laboratory, [‡]Ottawa Institute of Systems Biology, Department of Biochemistry, Microbiology and Immunology, University of Ottawa, Ottawa, Ontario, Canada

[§]Shanghai Institute of Materia Medica, Chinese Academy of Sciences, Shanghai, China

Supporting Information

ABSTRACT: Connexins are the structural subunits of gap junctions and act as protein platforms for signaling complexes. Little is known about tissue-specific connexin signaling nexuses, given significant challenges associated with affinity-purifying endogenous channel complexes to the level required for interaction analyses. Here, we used multiple subcellular fractionation techniques to isolate connexin32-enriched membrane microdomains from murine liver. We show, for the first time, that connexin32 localizes to both the plasma membrane and inner mitochondrial membrane of hepatocytes. Using a combination of immunoprecipitation-high throughput mass spectrometry, reciprocal co-IP, and subcellular fractionation methodologies, we report a novel interactome validated using null mutant controls. Eighteen connexin32 interacting proteins were identified. The majority represent resident mitochondrial proteins, a minority represent plasma membrane, endoplasmic reticulum, or cytoplasmic partners. In particular, connexin32 interacts with connexin26 and the mitochondrial protein, sideroflexin-1, at the plasma membrane. Connexin32 interaction enhances connexin26 stability. Converging bioinformatic, biochemical, and confocal analyses support a role for connexin32 in transiently tethering mitochondria to connexin32-enriched plasma membrane microdomains through interaction with proteins in the outer mitochondrial membrane, including sideroflexin-1. Complex formation increases the pool of sideroflexin-1 that is present at the plasma membrane. Together, these data identify a novel plasma membrane/mitochondrial signaling nexus in the connexin32 interactome.

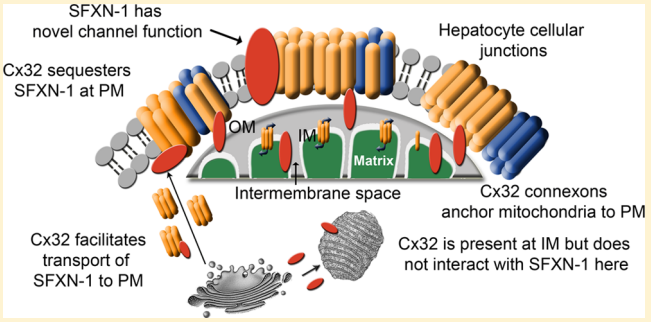

KEYWORDS: *gap junction, connexin, connexin32, connexin26, mitochondria, interactome, sideroflexin, mass spectrometry, immunoprecipitation, inner mitochondrial membrane*

INTRODUCTION

The formation of gap junction channels between two adjacent cells allows for direct cell−cell communication.[1] Functional diversity is dictated by their structural subunits, a family of 21 connexin proteins in humans.[2] Oligomerization of six connexins forms an aqueous pore when inserted into target membranes.[3] Each pore, known as a connexon or hemichannel, makes up one-half of a gap junction channel. In nonjunctional plasma membranes, connexons allow for regulated passage of ions and small molecules up to 1.8 kDa to and from the extracellular space.[3,4] In junctional plasma membranes, end-to-end docking of two apposing hemichannels enables gap junction intercellular communication (GJIC). Between adjacent membranes of the same cell, connexon alignments create reflexive junctions acting as conduits between membrane compartments (e.g., allowing for molecular traffic from perinuclear to adaxonal cytoplasm between processes of axon-ensheathing oligodendrocytes).[5] Signaling specificity is achieved by "mixing and matching" connexin subunits. Assemblies of identical (homotypic channels) or diverse pairings (heteromeric channels) define membrane channels with different permeabilities, gating properties, and docking compatibilities.[6]

Only recently have connexin-specific interacting partners been considered part of the gap junction protein signaling nexus. Connexin43 (Cx43), the most abundant and ubiquitously expressed connexin, has received the most attention with approximately 25 intracellular interactors identified (reviewed in refs 7,8). Transient extracellular Cx43−Cx43 (and Cx26−Cx26) interactions along extracellular docking domains also act as adhesive contacts, directing the migration of neural progenitor cells along radial glia.[9,10] Finally, connexin complexes can also form functional protein complexes in intracellular organelles. Using selected MS/MS ion monitoring validated by immunofluorescence, Cx43 has been identified in the inner mitochondrial membrane of cardiac myocytes.[11] Using classic biochemical methods, Cx32 has also been reported in hepatic mitochondria, but without further suborganelle localization.[11] MS methodologies, however, have

Received: December 12, 2012

dx.doi.org/10.1021/pr301166p | *J. Proteome Res.* XXXX, XXX, XXX−XXX

fallen short of the level of sensitivity required to explore these mitochondrial interactomes, given difficulties associated with purifying sufficient amounts of membrane-integrated connexin protein.

Mutations in Cx32 are the genetic determinant of X-linked Charcot-Marie Tooth Disease, a debilitating demyelinating peripheral neuropathy.[12] Loss of Cx32 (or depletion from the plasma membrane) enhances tumorigenesis in liver.[13−15] Here, to identify potential Cx32 interacting partners that may prevent hepatic disorders when complexed with Cx32, we enriched for connexin-specific membrane microdomains by subcellular fractionation,[11] and adapted our IP-high throughput mass spectrometry (IP-HTMS) methodology[16−18] to study endogenous integral membrane protein complexes. We show that Cx32 can be detected at both the plasma membrane and the inner mitochondrial membrane of healthy hepatocytes and interacts with plasma membrane, cytosolic, endoplasmic reticulum, and mitochondrial-resident proteins. Bioinformatic analysis, supported by confocal microscopy, provides further support for an intriguing role for Cx32 in transiently tethering mitochondria to plasma membrane microdomains.

MATERIALS AND METHODS

Generation of N15 C57BL/6 Cx32 Knockout (KO) and Congenic Wild-type (WT) Mice

Cx32 null mutant breeding pairs, kindly provided by Dr. Klaus Willecke (Universitat Bonn, Germany),[19] were backcrossed for 15 generations onto a C57Bl/6 background in the Bennett laboratory. Congenic WT mice were derived from heterozygote matings. Male mice used in this study were between 3 and 4 months of age. Genotyping was confirmed at time of weaning and again at time of sacrifice. PCR amplification was performed on a Whatman Biometra TGradient96 system. DNA, isolated from tail snips, was amplified using Primers A, B, and C (A: 5′-TCATTCTGCTTGTATTCAGGTGAGAGGCGG-3′, B: 5′-ATACACCTTGCTCAGTGGCGTGAATCGGCA-3′, C: 5′-TCTTACTCCACACAGGCATAGAGTGTCTGC-3′). Primer A (forward) and B (reverse) generate a 750 bp WT amplicon. Primer A (forward) and C (reverse) generate a 1300 bp KO amplicon. Primers were synthesized at Integrated DNA Technologies Inc. Cycling parameters were: 95 °C for 10 min, followed by 30 cycles of 95 °C for 60 s, 67 °C for 60 s, and 72 °C for 60 s. For all studies, liver was dissected and gall bladders removed from both WT and KO mice. For fractionation studies, tissue was processed fresh. For validation IP and Western analysis, tissue was frozen in liquid nitrogen and stored at −80 °C until required.

For measurements of ferritin, transferrin, iron, and total iron binding capacity, blood was collected by cardiac puncture from WT and KO mice (7 animals per genotype) between 1 and 8 months of age. Samples were clotted at RT for 1 h and centrifuged for 10 min at 1500× *g*. Recovered serum supernatant was sent on ice to the Charles River Research Animal Diagnostic Services Laboratory (Wilmington, MA). Transferrin saturation was calculated as the percentage of iron to total iron binding capacity.

Sucrose Gradient Fractionation

For each experiment, one liver lobe was homogenized in 1 mL PTN buffer (50 mM sodium phosphate, 1% Triton X-100 [T-8787, Sigma-Aldrich], 50 mM NaCl, pH 7.4, fresh protease inhibitor cocktail (10 mM DTT [Promega #V3151], 1 mM PMSF [OmniPure #7110], 5 μg leupeptin, [Pierce 78435], and 1 μg pepstatin A [Bioshop # PEP 605]) using a Teflon Potter-Elvehjem homogenizer fitted to a 30 mL glass tube. Homogenates were incubated on ice for 30 min and centrifuged at 12000 rpm for 3 min at 4 °C to remove nuclei. The Triton X-100 supernatant (containing the insoluble membrane fraction) was reserved on ice and diluted with an equal volume of 80% sucrose. Resulting homogenates (40% sucrose) were overlaid with equal volumes of 30% and 5% sucrose in Beckman polyallomer centrifuge tubes, (14 × 89 mm, #331372) and centrifuged at 32085 rpm (130000× g_{ave}) in an SW40 Ti swinging-bucket rotor overnight (18 h) at 4 °C. Gradients were carefully aliquoted (10 fractions of 500 μL) with fraction 1 being the uppermost, lightest fraction. Protein quantification was performed using the Bio-Rad DC protein assay kit (Bio-Rad, #500−0112).

Optiprep (OP) Purification of Liver Plasma Membrane and Mitochondria

Four livers per genotype (WT and KO) were dissected in ice-cold PBS (10 mM phosphate, 154 mM NaCl). PBS was decanted following collection and tissue weighed prior to being minced with scissors until homogeneous. Tissue pieces were washed with three changes of ice-cold Solution B (0.25 M sucrose, 1 mM EDTA, 2 mM $MgCl_2$, 20 mM HEPES-NaOH, pH 7.4). Five milliliters of solution B with fresh protease inhibitors (1 mM sodium fluoride [Sigma #S-1504], 50 μg/mL aprotinin [Sigma #A-6279], 1 mM sodium orthovanadate [Sigma #S-6508], 1 mg/mL PMSF) was added to the crude lysate at twice the volume per wet weight (g) of liver tissue (e.g., 5 mL buffer A per 2.5 g liver tissue). Lysates were homogenized using a tight-fitting dounce homogenizer and Teflon pestle (approximately 30 strokes). Lysates were transferred to 15 mL Falcon tubes and Solution B was added to fill the tubes prior to centrifugation at 3100 rpm (1561× g_{ave}) in a GH-3.8A rotor (Beckman-Coulter) at 4 °C for 10 min. The supernatant was collected with a Pasteur pipet, transferred to 1.5 mL polyallomer centrifuge tubes (Beckman #357448, with adaptors #355919), and centrifuged at 48,537 rpm (100000× g_{ave}) in a TLA100.3 rotor for 50 min. The supernatant (containing cytosolic proteins) was discarded, and the pellets were combined and resuspended in in a 35% OP solution (Sigma #D15556). The 35% OP solution was prepared by diluting a 50% working solution of OP in Solution B (50% working solution of OP: 5 parts OP with 1 part diluent [0.25 M sucrose, 6 mM EDTA, 12 mM $MgCl_2$, 120 mM HEPES-NaOH, pH 7.4]). Subsequent dilutions of OP were also prepared by diluting the 50% working solution with Solution B as above.

A discontinuous OP gradient was prepared on ice by slowly overlaying 2 mL of the resuspended pellets with 1 mL 30% OP, 2.5 mL each of 25% and 17.5% OP, and 2 mL each of 10%, and 2.5% OP solutions into 13.2 mL (14 × 89 mm) polyallomer centrifuge tubes. Solution B was added to a point one mm below the surface of the tube (~1 mL). Tubes were carefully balanced and adjusted with Solution B, if necessary, before assembly into an SW41 Ti rotor (Beckman Coulter). Gradients were centrifuged at 36555 rpm (165000× g_{ave}) at 4 °C for 3.5 h (acceleration = 1, deceleration = 0). The interfaces between the gradients were collected in 0.5 mL volumes by tube puncture. The collected interfaces were diluted with two volumes of Solution B and centrifuged in a TLA100.3 rotor for 50 min at 48500 rpm to collect the pellet. Pellets were resuspended in RIPA buffer (10 mM PBS, 1% NP-40, 0.5% sodium

dx.doi.org/10.1021/pr301166p | J. Proteome Res. XXXX, XXX, XXX−XXX

deoxycholate, 0.1% SDS) with fresh protease inhibitors (1 mM sodium fluoride, 50 μg/mL aprotinin, 1 mM sodium orthovanadate, 1 mg/mL PMSF) and assayed for protein concentration using the Bio-Rad DC protein assay kit.

Crude Mitochondrial Isolation

One liver per genotype was placed in ice-cold PBS. Tissue was minced with scissors and washed in PBS. Two volumes of buffer A (20 mM HEPES, 220 mM mannitol, 68 mM sucrose, 80 mM KCl, 0.5 mM EGTA, 2 mM magnesium acetate, 1 mM DTT, pH 7.4, and fresh protease inhibitors (1 mM NaF, 50 μg/mL aprotinin, 1 mM sodium orthovanadate, 1 mg/mL PMSF) were added and tissue homogenized in a dounce homogenizer with Teflon pestle until very smooth (about 30 strokes). The homogenate was centrifuged at 3000 rpm (738× g_{ave})in a JA25.50 rotor (50 mL tube) at 4 °C for 20 min. The supernatant was collected with a Pasteur pipet and transferred to a new tube for centrifugation at 8000 rpm (5251× g_{ave}) at 4 °C for 15 min. This supernatant was discarded and the pellet was washed with 30 mL of buffer A at 8000 rpm at 4 °C for 15 min as before. The mitochondrial pellet was resuspended in 1 mL buffer A.

Subfractionation of Mitochondria Following Sucrose Fractionation

Crude mitochondria were subjected to sucrose gradient fractionation with the following modifications: Mitochondrial samples were mixed with 80% sucrose to achieve a final concentration of 60% sucrose (4 mL total), and were overlaid with 50%, 40%, and 30% sucrose layers (2 mL each), followed by 2 mL homogenization buffer (minus DTT), and centrifuged at 35000 rpm (151263× g_{ave}) for 16 h at 4 °C. Twenty-four fractions of 500 μL each were collected. WT and KO fractions (WT, fractions 18−22; KO, fractions 17−21) were pooled and protein concentrations assayed using the Bio-Rad DC protein assay kit. Each set of pooled mitochondrial fractions were diluted 2:1 with cold buffer A. Mitochondria were pelleted by centrifugation at 8000 rpm for 15 min. Pellets were resuspended in cold buffer A and 0.6% digitonin (#D141, Sigma-Aldrich) and incubated on ice for 10 min to selectively permeabilize the outer mitochondrial membrane. Mitochondria were again collected by centrifugation at 10000× *g* for 10 min at 4 °C. The supernatant containing outer membrane proteins was reserved. Mitoplasts were resuspended in 150 mM KCl with fresh protease inhibitors and incubated on ice for 10 min prior to centrifugation at 10000× *g* for 10 min at 4 °C. The supernatant containing inner mitochondrial membrane proteins was reserved.

Endogenous Immunoaffinity Purification for HTMS

Anti-Cx32-coupled protein G agarose beads were prepared as follows: One mL of a protein G agarose bead slurry (1:1 PBS; Roche #20399) was incubated with 30 μg monoclonal anti-Cx32 antibody (CX32C13-M, Alpha Diagnostics) overnight at 4 °C. Beads were washed with 10 mL of 0.1 M borate buffer (pH 9.0) and resuspended in 10 mL of the same buffer. Anti-Cx32 antibody was chemically coupled to the protein G beads by the addition of solid dimethyl pimelimidate DMP (Pierce # D8388) to a final concentration of 20 mM. Beads were incubated for 30 min at room temperature. The cross-linking reaction was stopped by washing twice with 0.2 M ethanolamine (Sigma #E-9508, pH 8.2). Beads were resuspended in 10 mL of 0.2 M ethanolamine and incubated at room temperature for 2 h, followed by two washes with 10 mL of PBS. Beads were resuspended in PBS to a final volume of 1 mL and stored at 4 °C. One milligram of total protein of pooled sucrose fractions 4, 5, and 6 was used as input material for the 1× reaction. Five milligrams of total protein were used for the 5× reaction. The pooled fractions were diluted 1:2 in fresh RIPA buffer with protease inhibitors (1 mM sodium flouride, 50 μg/mL aprotinin, 1 mM sodium orthovanadate, 1 mg/mL PMSF) and precleared with 100 μL of uncoupled protein G agarose beads per 1 mL of protein lysate for 1 h at 4 °C. Precleared lysates (or an equal volume of RIPA buffer for the no lysate (NL) control) were added to either 400 μL (1× reaction) or 2 mL (5× reaction) anti-Cx32-coupled beads and incubated overnight at 4 °C. Beads were washed once in RIPA buffer with 250 mM NaCl, once in RIPA buffer with 125 mM NaCl, and three times in PBS (10 mM) for two minutes with gentle inversion. Proteins were eluted at room temperature for 30 min with inversion in one bead volume of ammonium hydroxide elution buffer (0.5 M NH_4OH, 0.5 mM EDTA). Samples were lyophilized in a SpeedVac and solubilized in 45 μL 2× SDS sample buffer (6× buffer diluted to 2× with 0.35 M Tris-HCl/0.28% SDS, pH 6.8 buffer [6× buffer: [0.35 M Tris-HCl/0.28% SDS, pH 6.8 buffer], and 5% glycerol, 10% SDS, 100 mM DTT, 0.002% bromophenol blue]) with 10% β-mercaptoethanol (BME) at room temperature for 30 min. The SDS-solubilized proteins were resolved on NuPAGE Novex 4−12% Bis-Tris gels (NP0335BOX, Invitrogen) at 100 V for 20 min, followed by 150 V until the dye front reached the bottom of the gel. Gels were fixed for 30 min in a 5% acetic acid/methanol solution and rinsed twice with double distilled water (ddH_20) for 2 min each. To minimize background, gels were washed in ddH_20 overnight with shaking at 4 °C, sensitized for 2 min in a 0.02% sodium thiosulfate solution, and rinsed twice for 30 s each with ddH_20. Fresh silver nitrate (0.1%) solution was incubated for 30 min, followed by two 30-s washes in ddH_20. Gels were developed with two changes of freshly prepared 0.01% formaldehyde in 2% sodium carbonate solution, rinsed with 1% acetic acid, and stored in the same solution at 4 °C.

HTMS Analysis

HTMS was performed as described[16−18] with the following modifications. Briefly, all surfaces in contact with the gel were wiped with 70% ethanol and precautions were taken to minimize contamination of gel and gel pieces with keratin and dust in air. Protein bands were excised on a clean glass plate with a #11 scalpel blade (blade was wiped with 70% ethanol before use, and changed between each band). Gel bands were cut into smaller pieces approximately 3 mm^2, transferred to 0.6 mL Eppendorf tubes, and washed by vortexing in 50 μL Solution A (50 mM ammonium bicarbonate [EMD #00113164]). The liquid was discarded following a brief centrifugation. Gel pieces were partially dehydrated in 50 μL Solution B (50% acetonitrile [ACN; J.T.Baker #9829−03], 25 mM ammonium bicarbonate) for 15 min at room temperature, centrifuged briefly, and the liquid was discarded. Samples were dried in a SpeedVac for 5 min without heating, followed by an incubation in 30 μL Solution C (50 mM ammonium bicarbonate, 10 mM DTT) for 15 min at 56 °C to rehydrate the gel pieces and reduce disulfide bonds. Tubes were cooled at room temperature for 15 min, centrifuged briefly, and the liquid discarded. To inhibit reformation of disulfide bonds, thiols were quenched by adding 30 μL Solution D (100 mM iodoacetamide [SIGMA #I1149] in 50 mM ammonium bicarbonate) in a 15 min incubation in the dark. Samples were centrifuged, washed

dx.doi.org/10.1021/pr301166p | J. Proteome Res. XXXX, XXX, XXX−XXX

Table 1. Primary Antibodies Employed

antibody[a]	catalogue number	source	type[b]	Western (μg/mL)	IP[c]	ICC (μg/mL)
ATP5A1	14676-1-AP	Proteintech Group	Polyclonal	0.2		
BiP (GRP78)	610979	BD Transduction	Monoclonal	2.0		
Cav-1	SC-894	Santa Cruz	Polyclonal	1.6		
Cx32	13-8200	Zymed, Invitrogen	Monoclonal			1
Cx32	CX32C13-M	Alpha Diagnostics	Monoclonal	0.5	1.25 μg/50 μL bead slurry	
Cx32	C3470	Sigma	Polyclonal	5.0		
Cx26	51-2800	Zymed, Invitrogen	Polyclonal	4.0	1.5 μg/50 μL bead slurry	
CoxIV	457325	Molecular Probes	Monoclonal	0.4		
Flot-1	610820	BD Transduction	Monoclonal	0.5		
Na^+K^+ATPase	05-369	Millipore	Monoclonal	0.5		
SFXN-1	12296-1-AP	Proteintech Group	Polyclonal	1.5	3.0 μg/50 μL bead slurry	2.5
VDAC1/Porin	ab15895	Abcam	Polyclonal	0.5		

[a]Abbreviations: ATP5A1, ATP synthase, H+ transporting, mitochondrial F1 complex, alpha subunit 1; BiP, heat shock 70 kDa protein 5 (glucose-regulated protein, 78 kDa); Cav-1, Caveolin-1; Cx32, Connexin32; Cx26, Connexin26; CoxIV, Cytochrome C Oxidase (Complex IV); Flot-1, Flotillin-1; Na^+K^+ATPase, Sodium−potassium adenosine triphosphatase; SFXN-1, Sideroflexin-1; VDAC1, Voltage-dependent anion-selective channel protein 1; IP, Immunoprecipitation; ICC, immunocytochemistry. [b]All monoclonal antibodies were raised in mouse. All polyclonal antibodies were raised in rabbit. [c]Bead slurry refers to a 1:1 ratio of protein G agarose beads and PBS.

in Solution A for 15 min, partially dehydrated in Solution B for 15 min, centrifuged briefly, and dried in a SpeedVac for 5 min without heating. Trypsin enzyme solution was prepared by adding 100 μL resuspension buffer to 20 μg porcine trypsin (Promega, #V5111) and mixing the resuspended enzyme with 310 μL of Solution A (sufficient for 10 samples). The enzyme solution was added to each sample at 28 μL/tube, incubated on ice for 10 min, excess solution removed and 10 μL of Solution E (25 mM ammonium bicarbonate) added to each tube incubated at 37 °C overnight. Samples were centrifuged briefly and the solution was transferred to a clean tube. Fifty microliters of Solution E was added to the gel pieces and incubated at room temperature for 20 min with occasional vortexing. Analytes were pooled with the other 10 μL of Solution E from the previous step. Peptides were extracted by incubating each sample in 50 μL of Solution F (5% formic acid [J.T. Baker #9832−03] and 50% ACN) for 20 min. The tubes were centrifuged and the peptide solution was pooled into the Solution E washes. Samples were lyophilized and stored at −20 °C.

LC−MS/MS was performed by dissolving the peptide samples in 5% formic acid and loading into a 200 μm × 5 cm precolumn packed in-house with 5 μm YMC ODS-A C18 beads (Waters, MA, #YMC086529) using a micro Agilent 1100 HPLC system (Agilent Technologies). Peptides were desalted online with 95% water (J.T. Baker #9831−03), 5% ACN, and 0.1% formic acid (v/v) for 10 min at 10 μL/min. The flow rate was split before the precolumn to produce approximately 200 μL/minutes flow at the column. Following elution, peptides were directed to a 75 μm × 5 cm analytical column packed with 5 μm YMC ODS-A C18 beads and eluted using a 1 h gradient (15 to 80% ACN with 0.1% formic acid) into a LTQ linear ion-trap mass spectrometer (Thermo-Electron, USA). MS/MS spectra were acquired in a data-dependent acquisition mode automatically selecting and fragmenting the five most intense peaks from each spectrum generated. Peak lists were generated from the MS/MS .raw file using Mascot Distiller 2.0.0.0 (Matrix Science) to produce .mgf files under default parameters with the exception that for each MS/MS peak, lists were generated assuming a 2+ and a 3+ charge. All .mgf files were analyzed and matched to the IPI database using the Mascot 2.1.04 database search engine (Matrix Science) with trypsin as digestion enzyme, carbamidomethyl of cysteine as a fixed modification, and methionine oxidation as a variable modification. Peptide and MS/MS mass tolerances were set at ±2 Da and ±0.8 Da, respectively, with 1 miss-cleavage tolerance and the significance threshold set to 0.01 ($p < 0.01$). Finally, an ion score cutoff of 30 was chosen to produce a false-positive rate of less than 1% in the MS data. The most logical assignment of the peptide in the database was reported, and when peptides matched to more than one database entry, only the highest scoring protein was considered. The network of proteins associating with Cx32 was arranged according to subcellular localization and visualized in an interaction network generated using the Osprey Network Visualization System (Osprey version 1.2.0; Samuel Lunenfeld Research Institute). Molecular functions and protein networks were analyzed using the Database for Annotation, Visualization and Integrated Discovery (DAVID) v6.7[20] and Ingenuity Systems Pathway Analysis software (IPA version 8.8, Ingenuity Systems Inc.).

Validation of Cx32 Interacting Partners by Coimmunoprecipitation (co-IP)

Validation of protein−protein interaction by co-IP was performed as described above with the following minor modifications: Protein G beads were coupled with monoclonal Cx32 or polyclonal antibodies (Table 1) directed against proteins identified by HTMS analysis. Input proteins for co-IPs were RIPA lysates of homogenized liver tissue. Livers were placed in borosilicate glass culture tubes (VWR, #47729−570) in 2 mL ice-cold RIPA buffer with fresh protease inhibitors. Tissue was homogenized using a variable speed Tissue Tearor (Biospec Products #985370−395) and passed through a 26-gauge needle 8−10 times to break up nuclei. Samples were incubated on ice for 20 min, and centrifuged at 16000 rcf for 30 min. Postnuclear supernatants were adjusted to 5 mg/mL protein with fresh RIPA buffer, and 1 mg of protein was used in each co-IP. Protein G agarose bead volumes were scaled down to 50 μL (antibody:bead ratio was maintained). In Figure 2C, 50 μg of input protein and 10 uL of Protein G agarose beads were used for the PM and mitochondrial IPs. No lysate (NL) controls were performed by substituting an equal volume of RIPA buffer for protein lysate. In Supplemental Figure 2, Supporting Information, the RIgG isotype control was performed in parallel to the WT, KO, and NL SFXN IPs,

dx.doi.org/10.1021/pr301166p | J. Proteome Res. XXXX, XXX, XXX−XXX

using 3.0 μg RIgG antibody/50 μL bead slurry, and 1 mg of WT protein lysate. Eluted, dried, and resuspended IP product was run on 12.5% Tris-HCl polyacrylamide gels (prepared in-house) and transferred to Immobilon PSQ PVDF membranes (Millipore, MA, # IPVH00010) for 60 min at 100 V or overnight at 22 V.

Immunoblotting

Liver isolated from WT and KO mice was homogenized in RIPA buffer containing protease inhibitors (1 mM NaF, 50 μg/mL aprotinin, 1 mM sodium orthovanadate, 1 mg/mL PMSF, 10 mM PBS). Alternatively, fractions and organelle separations described above were analyzed. Protein concentrations are indicated in each figure caption. Samples processed for Western analysis were diluted to a 1× final concentration using 6× SDS sample buffer (0.35 M Tris-HCl/0.28% SDS, pH 6.8, and 5% glycerol, 10% SDS, 100 mM DTT, 0.002% bromophenol blue) with 10% BME and solubilized at room temperature for 30 min. Samples subjected to IP and lyophilization were resuspended in 2× final SDS sample buffer. Proteins were resolved under reducing/denaturing conditions on 10% or 12.5% Tris-HCl polyacrylamide gels (prepared in-house) and transferred to Immobilon PSQ PVDF membrane at 100 V for 60 min. Membranes were blocked in 5% (w/v) skim milk powder-PBS (10 mM phosphate, 154 mM NaCl) with 0.1% Tween-20 (blocking buffer) for 1 h and incubated in primary antibody diluted in the same buffer overnight at 4 °C (Table 1). Membranes were rinsed twice in 0.1% PBST (10 mM phosphate, 154 mM NaCl with 0.1% Tween-20) and twice in blocking buffer for 10 min prior to a 1 h incubation in HRP-conjugated antimouse or antirabbit (Jackson ImmunoResearch Laboratories, Inc., PA; [antimouse #115-035-146; 1:2000] and [antirabbit #711-096-152; 1:5000]) secondary antibody diluted in blocking buffer. Signal was detected on X-ray film using SuperSignal West Pico Chemiluminescent Substrate (Pierce, #34808). Densitometry was performed using Image J v1.47b software (NIH). Data were expressed as the percentage of SFXN-1 normalized to Na^+K^+-ATPase localizing to either plasma membrane or mitochondrial membranes in KO samples relative to WT.

HEK293T Culture and Transfection of Human Cx32 Gene

HEK293T cells were maintained in Dulbecco's modified Eagle medium/F-12 (DMEM/F-12; Invitrogen #12400-024) with 10% fetal bovine serum (Invitrogen, #12483-020) and 1% penicillin/streptomycin antibiotic cocktail. The full cDNA coding sequence of the human Cx32 gene (Accession #: NC_000023) was cloned into the pcDNA6/V5-His B backbone (Invitrogen, #V220-01), and the empty vector was used as a negative control. HEK293T cells were plated in 6-well tissue culture plates on #1.5 glass coverslips (Zeiss #474030-9000-000). Four micrograms of plasmid DNA (human Cx32 or empty vector) and 10 μL of Lipofectamine 2000 reagent (Invitrogen, #11668-019) were each diluted in 250 μL warmed Opti-Mem reduced serum media (Invitrogen, #31985-088) and incubated for 5 min. The diluted plasmid and Lipofectamine solutions were gently mixed together and incubated for 20 min. The medium in each well was replaced with 1.5 mL warmed DMEM with serum (no antibiotic), and 500 μL of DNA:Lipofectamine complexes. Cells were incubated with transfection reagents overnight, and protein expression was allowed to proceed for 24 h.

Confocal Microscopy

Cells were washed with 10 mM cold tissue culture PBS, fixed with 3.7% formaldehyde/PBS for 10 min, and washed again in PBS. Fixed cells were incubated with monoclonal anti-Cx32 (1 μg/mL, #13−8200) and polyclonal anti-SFXN-1 (2.5 μg/mL) antibodies diluted in antibody buffer (10 mM PBS [10 mM phosphate, 154 mM NaCl], 3% BSA, 0.3% Triton-X, pH 7.2) overnight at 4 °C. Cells were washed 3× in 10 mM PBS for 5 min at room temperature, and incubated with Cy3 antirabbit IgG secondary antibody (1:800, Jackson ImmunoResearch Laboratories, Inc. # 711-166-152), and Atto488 antimouse IgG secondary antibody (1:1000, Alexis Biochem, #211-205TD-C100) in antibody buffer for 1 h at room temperature. Coverslips were washed 3× in 10 mM PBS for 5 min at room temperature, and mounted onto glass microscope slides using ProLong Gold antifade reagent (Invitrogen, #P36930). Colocalization was assessed by confocal laser scanning microscopy on a Leica TCS SP5 (Leica Microsystems) in z-stacks captured with Leica LAS AF software (version 2.41) using an HCX PL APO CS 63× 1.4 oil objective with a pinhole size of 1 Airy unit (or equal optical slices for multiple fluorophores).

RESULTS

Isolation of Cx32-Enriched Membrane Microdomains by Subcellular Fractionation

To enrich for membrane-integrated Cx32 microdomains, we used a modified lipid raft fractionation protocol to float triton-insoluble membranes in a sucrose gradient (Figure 1A). Given

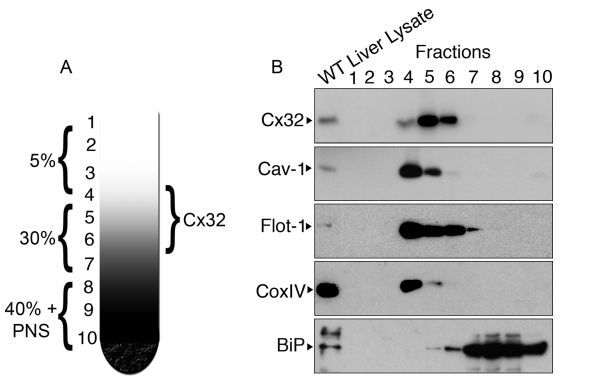

Figure 1. Cx32 is enriched in lipid rafts-containing membranes and mitochondrial membranes. (A) Sucrose gradient fractionation schematic for detergent-resistant membrane flotation. (B) Cx32 was detected in fractions 4, 5, and 6 using monoclonal anti-Cx32 (Table 1). Five micrograms of protein was loaded in each lane. Triplicate fractionations were performed. One representative analysis is shown.

connexin antibody cross-reactivity,[21] KO fractionations were performed in parallel to ensure specificity (Supplemental Figure 1, Supporting Information). In WT lysates, Cx32 was detected in fractions 4, 5, and 6 (Figure 1A,B). No labeling was observed in any of the KO fractions using the same monoclonal Cx32 antibody (Supplemental Figure 1, Table 1, Supporting Information). Fractions 4, 5, and 6 were located at the interface of 5% and 30% sucrose layers and in the lightest of the 30% sucrose gradients (Figure 1A). Fractions 4−6 were enriched for lipid raft markers caveolin-1 (Cav-1) and flotillin-1 (Flot-1) (Figure 1B, Table 1). Fractions 4 and 5 were also positive for inner mitochondrial membrane markers (cytochrome c oxidase

dx.doi.org/10.1021/pr301166p | J. Proteome Res. XXXX, XXX, XXX−XXX

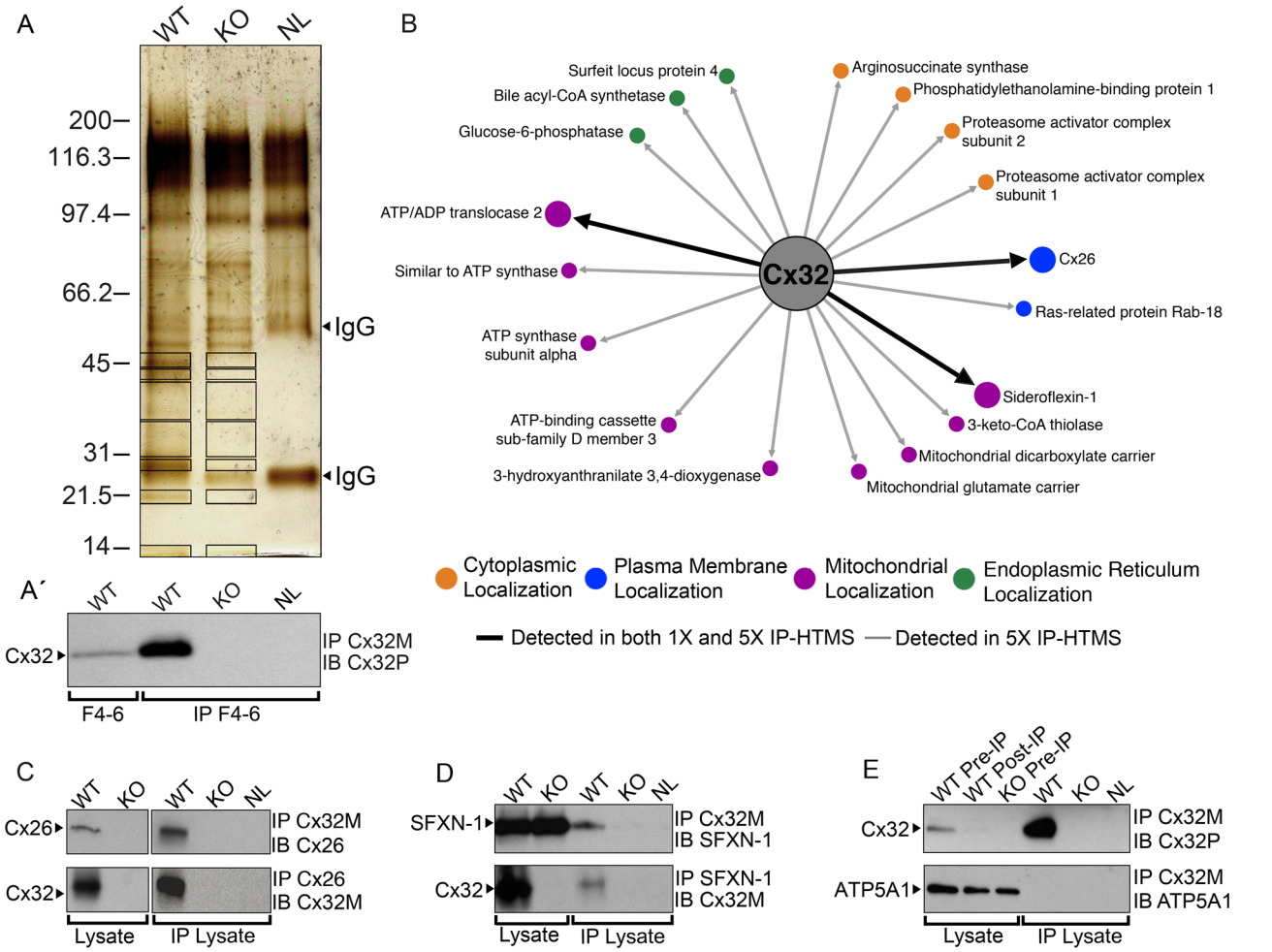

Figure 2. Identification of novel Cx32 interactors by IP-HTMS of Cx32-enriched liver membrane fractions and validation by co-IP of tissue lysates. (A) Silver stain of proteins found in sucrose gradient fractions 4−6 (Figure 1B) following IP with monoclonal anti-Cx32 (Table 1). Negative controls included IP reactions from KO fractions 4−6 (Supplemental Figure 1, Supporting Information) and a no lysate (NL) mock IP reaction. Black boxes indicate gel regions excised for tryptic digest. Mobility of precipitating IgG heavy and light chains are indicated by arrowheads. (A′) Western blot of Cx32-enriched fractions 4−6 (F4−6, 5 μg) and 1 μL (10%) of the corresponding IP products from these same fractions analyzed in (A). Analysis confirmed presence of bait (Cx32) in WT samples and lack of cross-reactivity in KO samples. Cx32-M indicates use of monoclonal anti-Cx32; Cx32-P indicates use of polyclonal anti-Cx32 antibody (Table 1). (B) IP-HTMS identified one known (Cx26) and 17 novel Cx32 interacting partners in replicate screens of 1 mg and 5 mg input protein. Interaction network generated by Osprey version 1.2.0 of proteins present in WT but not KO IP-HTMS. Proteins identified in both the 1 mg and 5 mg screens are represented with larger icons and thicker interaction lines than proteins identified only in the 5 mg screen. (C) Reciprocal co-IPs of liver lysates for Cx32 and Cx26. (D) Reciprocal co-IPs for Cx32 and SFXN-1. Specificity was also verified in independent IPs using an isotype IgG control (Supplemental Figure 2, Supporting Information). (E) IP for Cx32 and blotting for ATP5A1 did not validate a Cx32-ATP5A1 interaction.

subunit IV [CoxIV]) (Figure 1B and Table 1). The endoplasmic reticulum marker (heat shock 70 kDa protein 5 (glucose-regulated protein, 78 kDa) [BiP]) was detected at low levels in fractions 5 and 6 (Figure 1B and Table 1). Fractions 7−10 were devoid of Cx32 and enriched for BiP (Figure 1B and Table 1).

Identification and Validation of a Cx32 Interactome in Liver

Sucrose fractions 4−6 were pooled and incubated with monoclonal anti-Cx32 chemically coupled to protein G agarose beads (Table 1). WT Cx32 IP produced several bands that were visually absent in the KO purification in silver-stained gels, notably in the lower molecular weight range (Figure 2A, boxes, WT vs KO). A lysate-free reaction was also prepared by incubating Cx32-coupled beads in RIPA buffer only (Figure 2A, NL). Immunoblotting liver lysates or 10% of the Cx32 WT and KO IP input with polyclonal anti-Cx32 antibody (Table 1) demonstrated strong, specific enrichment of Cx32 in pooled immunopurified fractions (Figure 2A′, bottom panel compare WT F4−6 to WT IP F4−6 and KO, NL controls). Following excision of the unique silver-stained bands in WT and corresponding regions in KO lanes (Figure 2A, boxes), proteins were eluted from the gel pieces, digested with trypsin, and analyzed by LC−MS/MS. Table 2 presents Mascot scores, number of peptides, and the percent coverage for each protein identified from 5 mg of input protein (pooled liver fractions 4−6). Only proteins (a) with Mascot scores of 100 or higher in one or both paired analyses (b) for which at least two peptides were identified that were (c) absent from KO IP-HTMS analyses or (d) for which the same peptide was identified in IPs of both 1 mg and 5 mg WT protein fractions absent from KO met criteria to be included in the reported network (Table 2).

dx.doi.org/10.1021/pr301166p | J. Proteome Res. XXXX, XXX, XXX−XXX

Table 2. LC−MS/MS Identification of Cx32 and Binding Partners from Liver Tissue

			Mascot score	# of peptides	% coverage
IPI00118459	**Gap junction beta-1 protein (GJB1, Cx32)**	**Cell junction; Cell membrane; Gap Junction**	**160/370[a]**	**12/40[a]**	**10/21.2[a]**
IPI00125162	Gap junction beta-2 protein (GJB2, Cx26)	Cell junction; Cell membrane; Gap Junction	179/208[a]	4/15[a]	15/19.5[a]
IPI00115454	Sideroflexin-1 (SFXN-1)	Mitochondrion membrane; Ion transport	102/97[a]	1/1[a]	4/4[a]
IPI00127841	ADP/ATP translocase 2 (ANT-2, SLC25A5)	Membrane; Mitochondrion Transport	57/241[a]	1/5[a]	2.7/21.1[a]
IPI00313236	Bile acyl-CoA synthetase (SLC27A5)	Membrane; Endoplasmic Reticulum	441	8	14.5
IPI00226430	acetyl-Coenzyme A acyltransferase 2 (mitochondrial 3-oxoacyl-Coenzyme A thiolase) (ACAA2)	Membrane; Mitochondrion; Lipid metabolism; Fatty acid metabolism	396	7	30.2
IPI00133249	Surfeit locus protein 4 (SURF4)	Membrane; Endoplasmic Reticulum; Golgi Apparatus	301	4	20.8
IPI00130280	ATP synthase subunit α, (ATP5A1)	Mitochondrion inner membrane; ATP synthesis; Ion transport	228	4	7.6
IPI00135646	ATP-binding cassette subfamily D member 3 (ABCD3)	Membrane; Peroxisome Mitochondrion inner membrane; Transport	183	4	7.3
IPI00408961	3-hydroxyanthranilate 3,4-dioxygenase (HAD)	Cytoplasm; Pyridine nucleotide biosynthesis	176	3	11.9
IPI00124223	Proteasome activator complex subunit 1 (PSME1)	Proteasome	165	3	15.6
IPI00317074	Mitochondrial dicarboxylate carrier (SLC25A10)	Mitochondrion inner membrane; Transport	161	4	15.0
IPI00461407	similar to ATP synthase, H+ transporting, mitochondrial F1 complex, O subunit	Mitochondrion inner membrane	153	3	21.6
IPI00109275	Mitochondrial glutamate carrier 1 (GC-1, SLC25A22)	Mitochondrion inner membrane; Symport; Transport	145	3	11.1
IPI00134746	Argininosuccinate synthase (ASS1)	Amino acid biosynthesis; Arginine biosynthesis; Ligase	118	2	6.3
IPI00119645	Glucose-6-phosphatase (G6pc)	Endoplasmic reticulum; Gluconeogenesis; Carbohydrate Biosynthesis	111	2	8.4
IPI00137730	Phosphatidylethanolamine-binding protein 1 (PEBP1)	Cytoplasm; ATP/Lipid/Nucleotide Binding; Protease inhibitor	111	3	21.4
IPI00116770	Ras-related protein Rab-18 (RAB18)	Cell Membrane; Protein transport	110	2	10.7
IPI00124225	Proteasome activator complex subunit 2 (PSME2)	Proteosome	108	2	9.6

[a]Peptides detected in WT and not KO in two independent screens of 1 mg input and 5 mg input. Mascot scores and peptide coverage are reported only for both the 1 mg and 5 mg input screen separated by /. All other proteins were identified using 5 mg input only.

The complete list of proteins detected is provided as Supplemental Table 1, Supporting Information.

Eighteen interactors were identified (Figure 2B), including the known Cx32 binding partner, Cx26.[22] In total, 72% of the proteins identified by endogenous Cx32 IP-HTMS were intrinsic membrane proteins; 50% were mitochondrial resident proteins (Figure 2B). We validated by co-IP one plasma membrane (Cx26) and two inner mitochondrial membrane proteins, one novel (SFXN-1) and one predicted to be an artifact of detergent-insoluble sucrose fractionation (ATP5A1)[23] (Figure 2C−E). Tissue lysates were used instead of fractionated membranes to identify robust interactions. Both Cx26 and SFXN-1 reciprocally coimmunoprecipitated with Cx32 (Figure 2C,D). KO controls validated specificity of the interaction, which was further confirmed by immunoprecipitating WT protein using an isotype control rabbit IgG antibody (Chemicon (Millipore), #PP64). Only the SFXN-1 antibody specifically immunoprecipitated Cx32 (Supplemental Figure 2, Supporting Information). As expected,[23] we did not confirm a protein−protein interaction between Cx32 and ATP5A1 (Figure 2E) despite detection of Cx32 in the crude liver homogenates (pre-IP), effective immunoprecipitation (IP), and clearing of target protein from lysate post-IP (post-IP). ATP5A1 was detectable in both pre and post Cx32 IP as well as in the KO control (Figure 2E).

In addition to confirming antibody specificity and screening for nonspecific interactions, we also used Cx32 null mutant liver lysates to assess the effect of complex formation on the stability of validated Cx32 binding partners. Loss of Cx32 effectively reduced total Cx26 but not SFXN-1 protein levels in liver. Where immunoblotting for Cx26 produced a band at approximately 24 kDa in WT liver lysates, Cx26 was barely detected in Cx32 KO lysates (Figure 2C, top panel, lysate, Supplemental Figure 3, Supporting Information). Loss of Cx32 had no effect on overall levels of SFXN-1, detected as a single band at approximately 35 kDa (Figure 2D, top panel, lysate).

Cx32 Interacts with SFXN-1 at Both the Plasma Membrane and the Inner Mitochondrial Membrane

To explore the Cx32-SFXN-1 interaction, we sought to localize the Cx32-SFXN-1 complex with increasingly rigorous subcellular membrane fractionation techniques. Our initial IP-HTMS screen was performed by targeting Cx32 primarily integrated into plasma membrane lipid rafts. In this separation, however, lipid rafts partially cofractionate with mitochondrial membranes (Figure 1A). To separate plasma from mitochondrial membranes, we performed detergent-free fractionation of liver tissue using a discontinuous OP gradient (Figure 3A). In both WT and KO samples, plasma membrane markers (Na^+K^+-ATPase) were enriched at the 2−10% interface; the VDAC1/porin marker for outer mitochondrial membranes was detected

dx.doi.org/10.1021/pr301166p | J. Proteome Res. XXXX, XXX, XXX−XXX

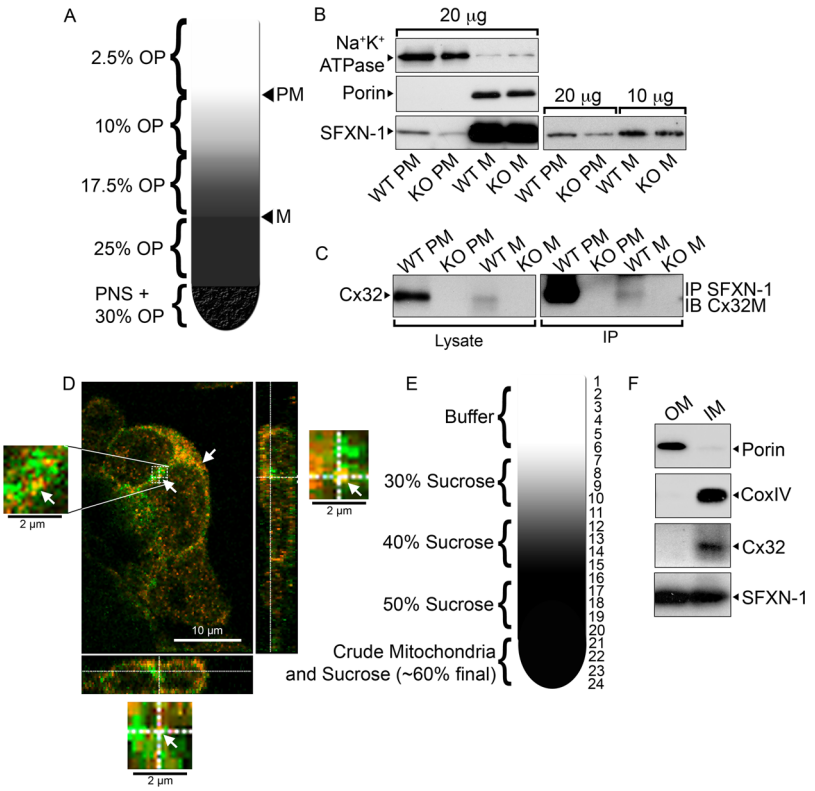

Figure 3. Cx32 interacts with SFXN-1 at plasma membrane. Loss of Cx32 reduces SFXN-1 levels at the plasma membrane. (A) Schematic of the OptiPrep (OP) gradient used to generate plasma membrane (PM) and mitochondrial membrane (M) fractions from WT and KO postnuclear supernatants cleared of cytosolic proteins. The plasma membrane fraction floated at the interface between the 2.5% and 10% OP gradient, while the mitochondrial fraction was found at the interface between the 17.5% and 25% OP gradient. (B) SFXN-1 localizes primarily to the porin-positive mitochondrial fractions with some SFXN-1 detected in Na^+K^+ATPase-positive plasma membrane fractions. SFXN-1 levels at the PM were reduced in KO compared to WT. A replicate purification is presented in the right panel with less mitochondrial protein loaded to highlight the observation that, in KO liver tissue, SFXN-1 is reduced only in the PM and not from the mitochondrial fraction. Quantitation is presented in Results. (C) Cx32 interaction with SFXN-1 is primarily detected at the PM but is also present in mitochondrial membranes following biochemical fractionation. (D) Confocal colocalization of ectopically expressed Cx32 (green) and endogenous SFXN-1 (red) in HEK cells transfected with human Cx32 suggests that *in situ* interaction is only detected at the plasma membrane at both junctional (insets and orthogonal views, arrow) and non junctional (arrow) membranes. (E) To further purify mitochondrial membranes from plasma membranes and subfractionate inner (IM) and outer (OM) mitochondrial membranes, sucrose gradient flotation was performed on crude mitochondria purified under detergent-free conditions. Twenty-four fractions were collected from both WT and KO samples. Fractions were assayed for expression of Cx32 and cellular fractionation markers (Supplemental Figure 5, Supporting Information). (F) In purified mitochondrial preparations, Cx32 localizes to IM; SFXN-1 localizes to both IM and OM.

at the 17.5−25% interface (Figure 3B, WT M, KO M). In two separate gradients, mitochondrial membrane contamination was never detected in plasma membrane fractions; low levels of Na^+K^+-ATPase, however, were consistently detected in mitochondrial fractions (Figure 3B, compare Na^+K^+-ATPase with porin-positive fractions). SFXN-1 was enriched in mitochondrial (M) but was also detected at lower levels in plasma membrane fractions (PM) (Figure 3B). This finding was further supported by the distribution of SFXN-1 across fractions 4−6 of our original detergent-resistant membrane sucrose gradient representing both plasma membrane and mitochondrial membranes (Supplemental Figure 4, Supporting Information).

Next, pooled plasma membrane (PM)-specific or mitochondrial (M)-specific fractions isolated from the OP gradient (Figure 3A) were immunoblotted for Cx32 (Figure 3C, left panel). As expected, Cx32 was enriched in plasma membrane fractions of WT samples (Figure 3C, left panel, WT PM). Low levels of Cx32, however, were also present in mitochondrial fractions (Figure 3C, left panel, WT M). Finally, we immunoprecipitated SFXN-1 from both plasma membrane and mitochondrial membrane fractions, and immunoblotted for Cx32 (Figure 3C, right panel). The interaction between these two proteins was strongest at the plasma membrane, but was also detectable in mitochondrial membranes (Figure 3C, right panel). KO controls confirmed specificity of Cx32 detection in both compartments (Figure 3C, left and right panels).

To rule out the possibility that this mitochondrial pool of Cx32 was not carry over from contaminating plasma membrane present in mitochondrial fractions, we purified crude mitochondrial preparations under detergent-free conditions, isolated contaminating plasma membranes from mitochondria by sucrose gradient flotation (Figure 3E, Supplemental Figure 5, Supporting Information), and separated the inner and outer mitochondrial membranes prior to Western blotting. As shown in Supplemental Figure 5, contaminating plasma membrane in our mitochondrial preparations was found in fractions 8−15 overlapping with fractions 13−16 enriched for CoxIV (Supplemental Figure 5). Fractions 17−23 represented pure mitochondria devoid of plasma membrane contamination in both WT and KO flotations (Supplemental Figure 5). Consistent with the OP gradients (Figure 3A-C), Cx32 was enriched at plasma membrane but was also clearly detectable in the mitochondria-only fractions (Supplemental Figure 5). A

dx.doi.org/10.1021/pr301166p | J. Proteome Res. XXXX, XXX, XXX−XXX

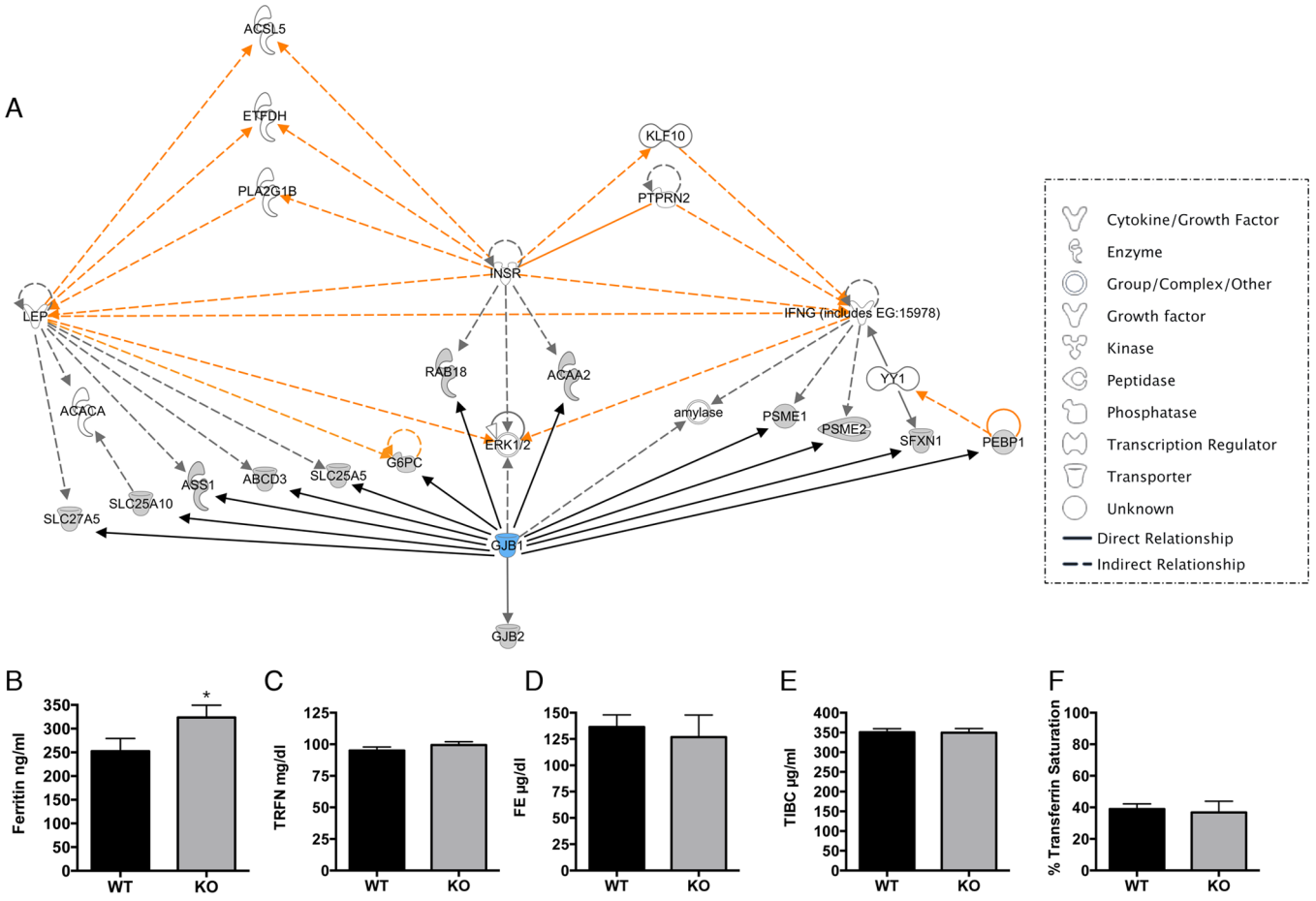

Figure 4. Ingenuity network analysis of the Cx32 protein interactome. (A) Proteins (listed by gene name) are represented as nodes (shapes indicate functional annotation). A documented biological relationship between two nodes is represented as a gray or orange edge (line). Gray edges represent interactions within a single network; orange edges cross-link nodes from multiple interacting networks. Proteins identified in our screen are represented as gray nodes with black edges (lines). White nodes represent gene products that participate in these networks, but were not identified in this study. Interactors that are not implicated in these primary networks are not included. The direct Cx26−Cx32 interaction validated in our screen is a known interaction and thus appears as a gray edge. All gray and orange edges are supported by references maintained by the Ingenuity Pathways Knowledge Base. Solid gray edges represent direct interactions; indirect interactions are represented by dashed lines. Circular lines describe a feed-back loop wherein a node has been shown to self-regulate. (B) Serum analysis of blood collected from WT and KO animals reveals that KO animals exhibit mild hyperferritinemia, without concurrent changes in serum transferrin (C) iron (D), total iron binding capacity (E), or % transferrin saturation (F).

biologically relevant interaction between Cx32 and SFXN-1 would require that both interacting partners be present in the same mitochondrial membrane compartments. Outer mitochondrial membranes (OM) were further isolated from pooled fractions 17−23 using a 0.6% digitonin solubilization protocol. Inner mitochondrial membranes (IM) in remaining mitoplasts were osmotically disrupted in a 150 mM KCl solution and collected by centrifugation. The OM sample was enriched in VDAC1/porin and devoid of CoxIV (Figure 3F). The IM sample was enriched in CoxIV and devoid of VDAC1/porin (Figure 3F). Mitochondrial Cx32 localized exclusively to the IM. SFXN-1 was found equally distributed across both OM and IM compartments (Figure 3F).

While these data clearly show that Cx32 and SFXN-1 are detected at both PM and IM, biochemical fractionation cannot rule out an exchange of interacting proteins from different compartments postlysis. To address this, we localized *in situ* Cx32-SFXN-1 interactions by confocal microscopy in human Cx32-transfected HEK cells (Figure 3D). Cx32 (green) puncta overlap with the SFXN-1 (red) signal at both junctional membranes (arrows), and nonjunctional membranes (arrows). Colocalization was observed at the cytoplasmic face of the plasma membranes. This staining pattern is consistent with the hypothesis that Cx32 in gap junctional plaques at plasma membrane can interact with SFXN-1 at the plasma membrane and/or between apposed plasma and outer mitochondrial membranes, but not with the hypothesis that the interactions can occur at the inner mitochondrial membrane (Figure 3D).

To explore consequences of this PM-OM interaction, we asked whether SFXN-1 localization was influenced by its interaction with Cx32. We compared SFXN-1 levels in both mitochondrial and plasma membrane compartments of WT and KO liver. We found that localization of SFXN-1 at the plasma membrane, but not at inner and outer mitochondrial membranes, was reduced by 54 ± 17% in KO liver as determined by densitometry of replicate independent fractionations compared to WT (100%) (Figure 3B). This change represented a shift in subcellular localization (Figure 3B) without altering total SFXN-1 levels (Figure 2D) suggesting that plasma membrane Cx32 likely interacts with SFXN-1 resident in outer mitochondrial membrane and that detection of SFXN-1 at plasma membrane may represent a subpool of

dx.doi.org/10.1021/pr301166p | *J. Proteome Res.* XXXX, XXX, XXX−XXX

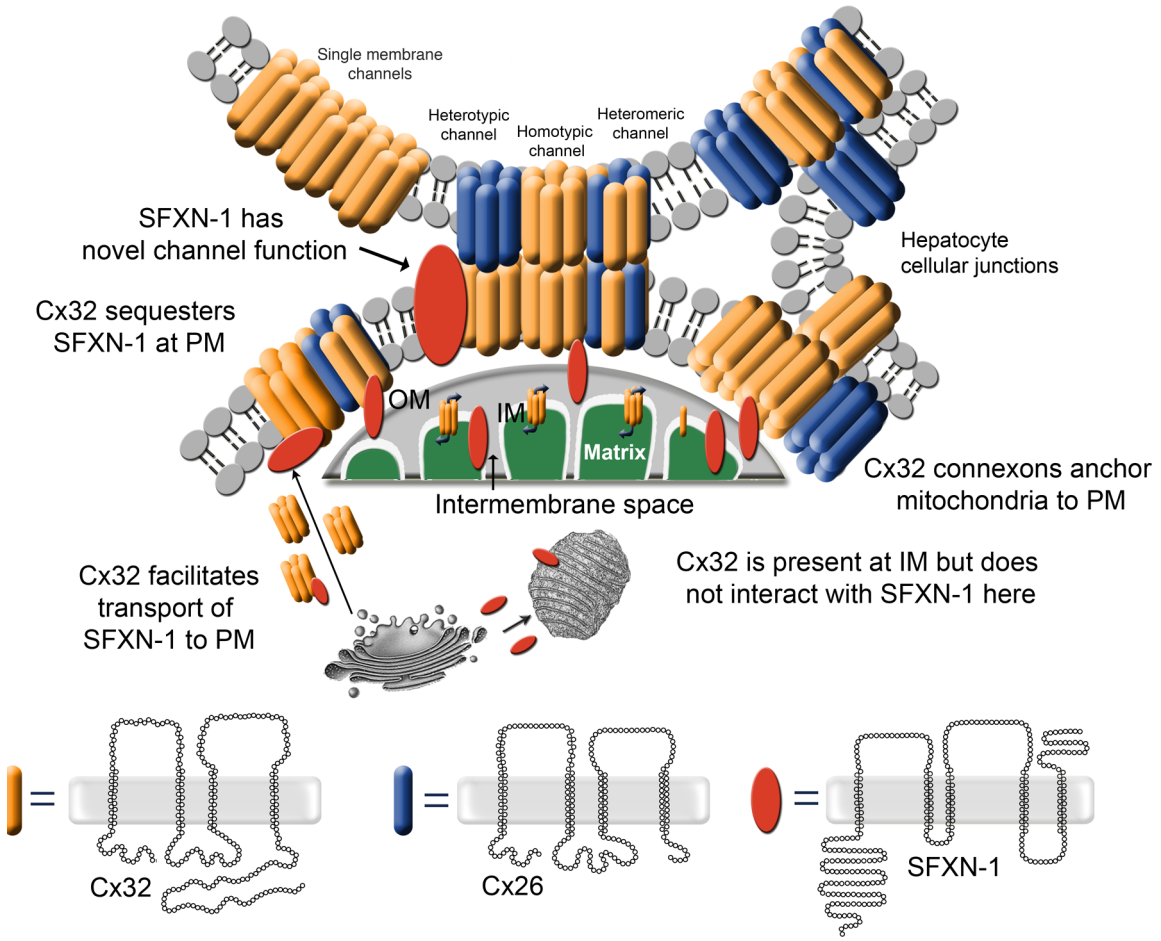

Figure 5. Schematic of hepatic gap junctions showing possible sites of Cx32-SFXN-1 interaction. Cx32 (orange) forms heterotypic and heteromeric gap junction channels with Cx26 (blue). Cx32 is also present on inner mitochondrial membranes. SFXN-1 (red) is present on both outer and inner mitochondrial membranes, and possibly at plasma membrane. Sites of Cx32-SFXN-1 interaction include (1) plasma membrane gap junctional plaques either as (i) transient interactions, (ii) novel plasma membrane resident proteins, (iii) part of the docking mechanism tethering subplasmalemmal mitochondria to the plasma membrane, or (iv) to promote the transport of small molecules into mitochondria, and (2) the inner mitochondrial membrane (unknown role).

SFXN-1 removed from apposing mitochondrial membranes during co-IP without affecting total cellular levels.

Network Analysis of Dual Plasma Membrane/Mitochondrial Cx32 Interactomes

Taken together, the interaction of Cx32-SFXN-1 at the plasma membrane, and reciprocal localization at the inner mitochondrial membrane suggested the presence of overlapping organelle-specific Cx32 protein networks in liver. To explore the nature of these networks, we performed functional annotation clustering using DAVID[20] and protein interaction network analysis using Ingenuity Systems Pathway Analysis software (Figure 4). Cx32 interactors clustered into two main functional classifications: (1) drug metabolism, lipid metabolism, molecular transport and (2) endocrine system development and function, molecular transport, cellular development. Pathway analysis identified three overlapping pathways implicated in (1) liver metabolic response to adipose-derived leptin, (2) liver response to insulin/insulin receptor signaling, and (3) interferon gamma responsiveness/iron metabolism impaired in hepatic carcinoma (Figure 4A). Dysfunction in leptin and insulin pathways, potentially mediated through disruptions in Cx32 interactions with SLC27A5, SLC25A10, ASS1, ABCD3, SLC25A5, and GP6 (Figure 4A) is consistent with previous reports that C57BL/6x129/SV Cx32 null mutant mice exhibit a small reduction (~17%) in body weight[19] also observed in our colony backbred to a pure C57BL/6 lineage (data not shown). Proposed regulation of interferon gamma responsiveness/iron metabolism by a Cx32 interactome with SFXN-1, PMSE1, PMSE2, and PEBP-1 (Figure 4A) is, however, novel. To test directly whether Cx32 KO mice show any dysfunction in these pathways, we measured circulating ferritin (Figure 4B), transferrin (Figure 4C), iron (Figure 4D), total iron binding capacity (Figure 4E), and percent transferrin saturation (Figure 4F). Cx32-null mutant mice exhibited a mild, significant hyperferritinemia (Figure 4B) without any indication of systemic iron overload (Figure 4C–E) or changes in transferrin saturation (Figure 4F). Taken together, this phenotype is consistent with hyperferritinemia observed following liver injury and as a result of systemic inflammatory conditions.[24]

DISCUSSION

Here, we report a novel endogenous Cx32-interacting network in mouse liver identified by immunoaffinity purification of Cx32-enriched subcellular membrane microdomains. Using unbiased IP-HTMS, we mapped 18 interacting partners. Fifty percent were resident mitochondrial proteins, 22% were

dx.doi.org/10.1021/pr301166p | J. Proteome Res. XXXX, XXX, XXX–XXX

cytoplasmic proteins, 17% localize to the endoplasmic reticulum, and 11% were predicted to be resident in plasma membrane. By reciprocal co-IP, subcellular fractionation, and confocal microscopy, we found that Cx32 forms protein−protein complexes at the plasma membrane (i.e., with Cx26) and either sequesters SFXN-1 at the plasma membrane or forms protein−protein complexes between Cx32 and SFXN-1 resident in apposing plasma membranes and outer mitochondrial membranes. Bioinformatic analysis places these interactions into three overlapping networks: (1) liver metabolic response to adipose-derived leptin, (2) liver response to insulin/insulin receptor signaling, and (3) interferon gamma responsiveness/iron metabolism. The observation that Cx32, integrated into plasma membrane, can interact with resident outer mitochondrial membrane proteins further suggests a novel role for connexins in possibly transiently tethering mitochondria to connexin-enriched plasma membrane domains (Figure 5). Together, these data highlight a novel plasma membrane/mitochondrial signaling nexus mediated by the Cx32 interactome.

This study represents the first endogenous connexin network mapped by unbiased MS approaches. The majority of reported connexin interactors have been identified using ectopically expressed tagged proteins, or exogenous peptides as "bait".[7,8,25] Endogenous partners have been inferred primarily from careful immunofluorescence colocalization studies.[7,8,25] These data have provided essential insight into channel-independent connexin function, notably for Cx43,[7,8,25] however, tissue-specific network analyses are lacking. To our knowledge, only two MS-based proteomic screens have been performed, both using a C-terminal fragment of Cx43 as bait.[26,27] The primary obstacle has been the challenge associated with affinity purifying endogenous membrane channel complexes in sufficient amounts for MS detection. To address this, we enriched for Cx32-positive membrane microdomains by subcellular fractionation prior to IP-HTMS. Cx32 null mutant controls were used to identify and eliminate background interactors. Success of this strategy was validated by the fact that our top 'hit' was the known Cx32 binding partner, Cx26.[22] Cx26 and Cx32 have been shown to colocalize in heterotypic (and presumably heteromeric) channels in liver hepatocytes.[22] Moreover, we also find that Cx26 protein levels are reduced in liver of Cx32 KO mice, consistent with earlier reports.[22] This reduction is likely due to a loss of Cx26 protein stability in absence of Cx32/Cx26 complexes, as steady-state Cx26 mRNA levels in WT and KO liver are comparable.[19]

Certainly, further improvements can be made to increase identification of connexin-interacting proteins by IP-HTMS. We have recently developed a gel-free centrifugal proteomic reactor to analyze membrane proteins[28] and have begun to adapt this technology to analyze fractionated membrane microdomains enriched in Cx32. Our centrifugal proteomic reactor is a simplified, user-friendly, adaptation of gel-free digestion. We exploit the fact that most proteins are positively charged at pH <3 and thus a protein/trypsin mixture will bind tightly to a small volume of strong cation exchange (SCX) beads while nonionic detergents and contaminants are readily washed away.[28] We then use DTT and iodoacetamide for protein reduction and alkylation, activate the trypsin by increasing pH to 8, and elute the resulting peptides in alkaline buffer for LC−MS/MS analysis.[28] Using this gel-free methodology, we have been able to detect 945 plasma membrane proteins and 955 microsomal membrane proteins in hepatic cells.[28] More than 800 out of these 945 and 955 proteins were not identified by the conventional in-gel digestion approach.[28] We anticipate that these improvements will further expand upon this study's identification of a mitochondrial protein-connexin interactome. Application will require further optimization as we have found that the phospholipid-Cx32 interactions[29] in our fractionated microdomains complicate the required pH-dependent binding to cationic beads. Despite clear presence of Cx32 in IP samples, detection of bait connexins by HTMS has not been consistent using the centrifugal reactor.[28] We are currently exploring the efficacy of mild cross-linking followed by delipidation to circumvent this problem and increase the number of connexin binding proteins we can identify.

Despite the fact that we may be able to identify more interacting partners in future, we report here that the majority of novel Cx32 interactors detected were resident mitochondrial proteins. In previous targeted approaches, plasma membrane and cytoplasmic proteins predominate in connexin complexes. In rat hepatocytes, Cx32 has been shown to colocalize with the tight junction proteins occludin and claudin-1, and the scaffolding protein zona occludens-1.[30,31] In the brain, oligodendrocytic Cx32 colocalizes with ZO-1 and the ZO-1-associated nucleic acid-binding protein.[31] In lipid rafts, Cx32 interacts with caveolin-1, the ubiquitously expressed calcium binding protein, calmodulin, and the membrane-associated guanylate kinase family member, Discs large homolog-1 (Dlgh-1).[32−34] Cx32 presumably sequesters Dlgh-1 at the plasma membrane as acute removal enables its translocation to the nucleus.[34] Here, we show that the Cx32-SFXN-1 interaction may have a similar effect with Cx32 sequestering a subpool of the resident mitochondrial protein SFXN-1 to the plasma membrane. Comparison of our quantitative biochemical analyses and confocal localization studies, however, suggests that the primary function of the Cx32-SFXN-1 interaction is likely not to regulate localization of binding partners. First, *in situ* interaction with SFXN-1 at the plasma membrane as assessed by confocal microscopy is not ubiquitous in Cx32-overexpressing HEKs. Second, unlike the effect of Cx32 null-mutation on Cx26 stability, overall SFXN-1 protein levels are not significantly altered, nor is mitochondrial subcellular localization determined by biochemical assessment in Cx32 KO liver lysates. Rather, by confocal assessment in HEKs ectopically expressing human Cx32, small, regionally distinct pools of SFXN-1, apparently at the outer mitochondrial membrane, colocalize with plasma membrane-resident Cx32. In null mutant liver lysates, SFXN-1 levels at plasma membrane are quantitatively reduced compared to WT, as determined by direct biochemical assay and mass spectrometry. Taken together, these observations provide tantalizing support for the emerging hypothesis that connexins may transiently tether mitochondria to the plasma membrane when binding partners come into apposition,[35] further supported by evidence that analagous complex associations with Cx43 are transient, yet strong enough to be coimmunoprecipitated.[36]

Despite this evidence, we were mindful that mitochondrial contaminants routinely copurify with detergent-resistant lipid raft preparations and are often misinterpreted as *bona fide* interactors.[23] Spurious interactions with F(1)/F(0) ATPase subunits and voltage-dependent anion selective channels are common.[23] Here, we used co-IP and bioinformatic analyses to rule out Cx32 interactions with the ATPase subunit ATP5A1 and the unidentified protein similar to ATP synthase, H+

dx.doi.org/10.1021/pr301166p | J. Proteome Res. XXXX, XXX, XXX−XXX

transporting, mitochondrial F1 complex, O subunit identified in our IP-HTMS screen. We show definitively that ATP5A1 does not co-IP with Cx32. Moreover, F(1)/F(0) ATPase subunits are not predicted to participate in the three main pathways identified by Ingenuity Pathway analysis. Our validation, however, of SFXN-1-Cx32 complexes at both plasma and mitochondrial membranes is consistent with a previous report that Cx32 is present in isolated liver mitochondria.[11] Indeed, Cx43 is certainly capable of translocating to the inner mitochondrial membrane of cardiomyocytes,[11] where Cx43 channels protect cells from excitotoxic insult.[37−40] It is, however, important to note that in this study, while we have biochemical evidence indicating that Cx32 and SFXN-1 are both present in inner mitochondrial membranes, we do not have evidence to suggest that an interaction occurs at this location. *In situ* imaging indicates that the primary interaction between these two proteins occurs between plasma membrane-localized Cx32 and outer mitochondrial membrane SFXN-1. Thus, while our data is the first demonstration that Cx32 is present at inner mitochondrial membranes, we must conclude that the low level Cx32-SFXN-1 interaction detected by IP in isolated mitochondrial membranes is likely due to contamination of these fractions with trace amounts of plasma membranes as shown in our data. Given that intracellular interactions between Cx32 and SFXN-1 were rarely detected in our HEK cell transfectants, we favor the hypothesis that the interaction seen in tissue lysates is due to transient interactions of outer mitochondrial membrane SFXN-1 with Cx32-containing gap junction plaques.[41]

SFXNs are an evolutionarily conserved family of mitochondrial tricarboxylate carrier proteins.[42−44] SFXN-1 is a five-membrane spanning integral membrane protein predicted to be either a channel or carrier protein. Mutations in SFXN-1 are the genetic determinant of transient embryonic and neonatal anemia presented in the *flexed-tail (f/f)* mouse model,[45] wherein defects in iron metabolism lead to a transient iron overload and intramitochondrial iron deposits in erythrocytes.[45] Interestingly, presentation of iron defects coincides with the onset of hepatic erythropoiesis, and persists through postnatal day 7 subsiding between the second and third week postnatal.[45] This time course corresponds closely with the developmental increase in hepatic Cx32 levels that do not reach adult levels until postnatal day 21.[46] Iron overload has been shown to reduce the presentation of Cx32 at plasma membrane in favor of intracellular distribution.[47] Thus, iron deficits in SFXN-1-deficient mice may promote the mitochondrial localization of Cx32, although this hypothesis remains to be tested. Here, we asked the reverse question: What effect does Cx32 null mutation have on ferritin status and iron metabolism? Based on the predicted involvement of Cx32 protein−protein interactions with the interferon gamma response in hepatocytes, we highlight a novel regulation of isolated hyperferritinemia observed in the absence of iron overload, that is characteristic of dysregulated chronic inflammatory responses.[24] Ferritin elevations are seen in a number of liver disorders including alcoholic and nonalchoholic steatohepatitis, viral hepatitis, and acute liver injury.[48] Moreover, elevated ferritin levels are associated with insulin resistance and purported to be the hepatic manifestation of metabolic syndrome.[48] Our data implicate the connexin-interacting nexus identified here in leptin, insulin, and interferon gamma signaling pathways. Interestingly, these pathways also link the Cx32 interactome identified in this study to the regulation of liver tumorigenesis.[13,14,49,50] For example, the interactions between Cx32 and the mitochondrial solute carrier proteins SLC25A10 and SLC25A5 as well as one of rate-limiting synthases in the arginine biosynthesis pathway (Ass1) are predicted to underlie the metabolic response to leptin in hepatocytes, notably in the exchange of citrate for malate between cytosol and mitochondria required for fatty acid synthesis, lipogenesis, and the regulation of protein catabolism, ammonia levels, and nitric oxide generation.[51,52] Cx32 interaction may act to stabilize membrane presentation, as shown here and by others for Cx26,[19] given that both Cx32 and SLC25A5 are downregulated in human heptatocellular carcinomas.[14,53] Certainly, mutations in ASS1 that impair protein stability are known causes of citrullinemia type I leading to liver failure, as well ethanol-induced liver injury.[52,54] This pathway analysis is consistent with previous reports that Cx32 null mutant mice are mildly underweight compared to controls.[19]

Further, given that SFXN-1 likely facilitates transport of components, notably pyridoxine, required for iron utilization into and out of the mitochondria,[45] its function may depend upon a network of channel transporters moving required components through plasma membrane to mitochondria. The interaction of Cx32 at the plasma membrane and SFXN at the outer mitochondrial membrane could serve to tether a pool of subplasmalemmal mitochondria to the plasma membrane, and potentially facilitate transport of pyridoxine into the mitochondria. In support of this hypothesis, another Cx32 interactor identified in this study, ANT-2, has been shown to function as both a mitochondrial and plasma membrane translocase.[55−58] Moreover, the known Cx32 interactor caveolin-1 also binds to the ABCD transporters,[59] and our identification of a potential Cx32-ABCD3 interaction, possibly including caveolin-1 in complex, provides further support for the idea that Cx32 participates in the tethering of mitochondria to lipid raft domains. As Cx32 localizes to the basolateral membrane domains of hepatocytes wherein the majority of transporters are located,[60] these interactions would presumably enable transient mitochondrial docking at site of metabolic import (Figure 5). Similar functional interactions have been described in developing muscle cells between the L-type calcium channel $\alpha 2/\delta 1$ subunit and the ATP5B subunit of the mitochondrial ATP synthase complex.[61]

In summary, this work describes the identification of a network of liver-specific Cx32 interacting proteins enriched in mitochondrial targets. These interactions were validated by co-IP and detergent-free subcellular fractionation, and provide evidence for a novel signaling nexus made possible by Cx32 interactions with resident proteins at plasma and mitochondrial membranes that are implicated in liver function and hepatocyte growth, differentiation, and tumor progression.

■ ASSOCIATED CONTENT

Supporting Information

Supporting figures and materials. This material is available free of charge via the Internet at http://pubs.acs.org.

■ AUTHOR INFORMATION

Corresponding Author

*D.F.: dfigeys@uottawa.ca, Tel. (613) 562-5800 x 8674, Fax (613) 562-5452. S.A.L.B.: sbennet@uottawa.ca, Tel. (613) 562-5800 x 8372, Fax (613) 562-5452.

Supplemental Figure 1: Cx32 is not detected in KO sucrose gradient fractions. To exclude non-specific interactors and confirm monoclonal antibody specificity (Table 1), KO liver tissue was fractionated as in Figure 1. CoxIV was used to confirm protein integrity in fractions 4-6. Note that the Cx32 lysate presented was immunoblotted at the same time and analyzed at the same exposure as the Cx32 fractions.

Supplemental Figure 2: Independent validation of SFXN-1 and Cx32 co-IP with Isotype IgG control. IP for SFXN-1 and blotting for Cx32 in WT and KO liver lystatse confirmed interaction not present following IP of WT liver lysate using a rabbit IgG isotype control.

Supplemental Figure 3: Cx26 protein levels are reduced in Cx32 KO liver. Cx26 levels are lower in KO compared to WT liver (see also Figure 2C). Actin was used as a loading control to confirm protein integrity.

Supplemental Figure 4: SFXN-1 co-fractionates with Cx32. Detergent-resistant membranes from the sucrose gradient depicted in Figure 1A were immunoblotted for SFXN-1. SFXN-1 overlaps with Cx32 (Figure 1A) in fractions 4-6. Antibodies are listed in Table 1.

Supplemental Figure 5: WT and KO sucrose flotation of crude mitochondrial preparations. (A) WT. (B) KO. Contaminating Na^+K^+ATPase-positive plasma membrane is detected in fractions 10-15 (WT) and 9-15 (KO) of crude WT mitochondria separated by sucrose gradient (Figure 3D). CoxIV-postive mitochondrial membranes overlap with fractions 13-16. Pure CoxIV-positive mitochondrial membranes are enriched in fractions 17-22 (WT) and 17-21 (KO). Cx32 is primarily detected in plasma

membrane fractions but clearly present in mitochondrial fractions devoid of any plasma membrane contamination. KO controls confirm monoclonal Cx32 antibody specificity (Table 1).

Supplemental Table 1: Complete list of all proteins detected by IP-HTMS (excel file)

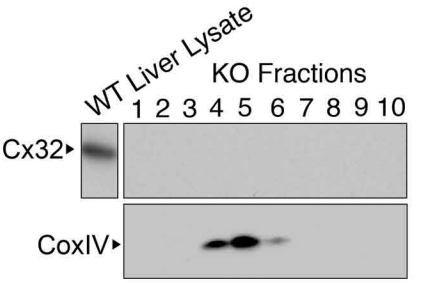

Supplemental Figure 1

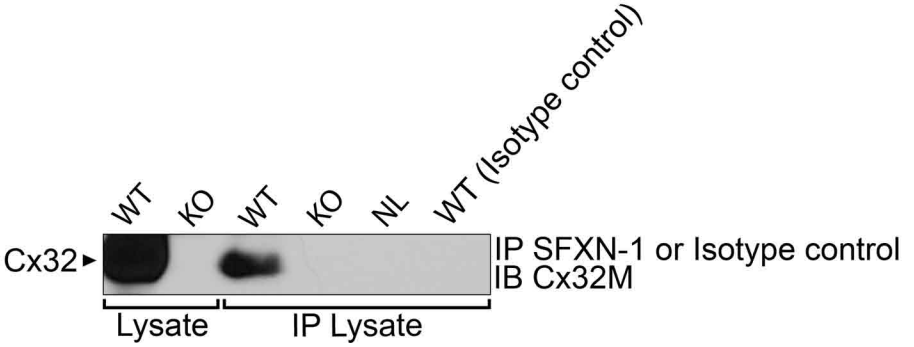

Supplemental Figure 2

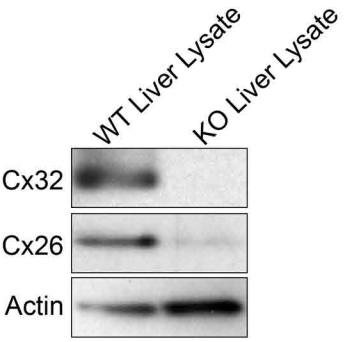

Supplemental Figure 3

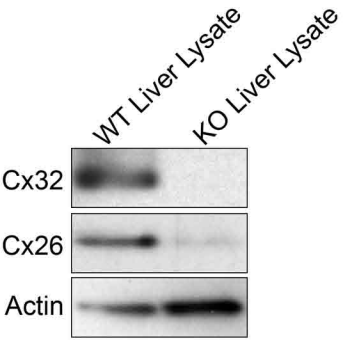

Supplemental Figure 3

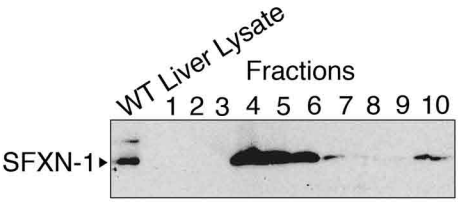

Supplemental Figure 4

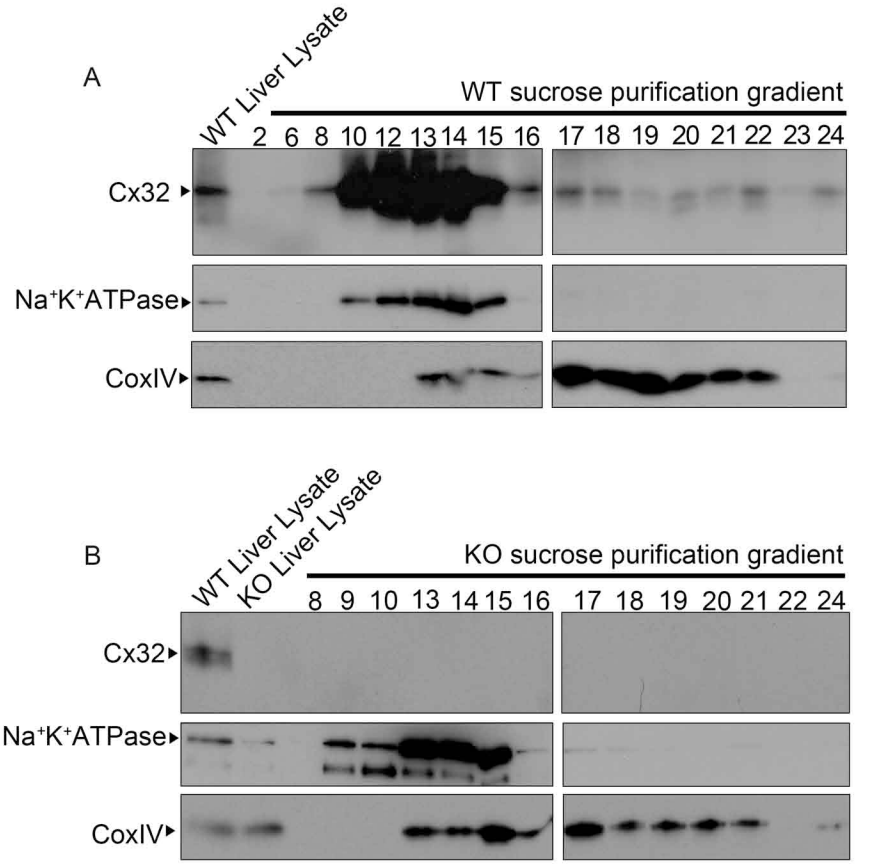

Supplemental Figure 5

Notes

The authors declare no competing financial interest.

■ ACKNOWLEDGMENTS

This work was funded by CIHR (MOP 62826) to S.A.L.B., O.G.I. and the CIHR Training Program in Neurodegenerative Lipidomics (CTPNL) (TGF 96121) to S.A.L.B. and D.F. S.F. received a CIHR Banting and Best doctoral award. H.Z. and M.A. were supported by the Institute of Aging and CTPNL.

■ REFERENCES

(1) Simon, A. M.; Goodenough, D. A. Diverse functions of vertebrate gap junctions. *Trends Cell Biol.* **1998**, *8*, 477−83.
(2) Willecke, K.; Eiberger, J.; Degen, J.; Eckardt, D.; Romualdi, A.; Guldenagel, M.; Deutsch, U.; Sohl, G. Structural and functional diversity of connexin genes in the mouse and human genome. *Biol. Chem.* **2002**, *383*, 725−37.
(3) Stout, C.; Goodenough, D. A.; Paul, D. L. Connexins: functions without junctions. *Curr. Opin. Cell Biol.* **2004**, *16* (5), 507−12.
(4) Neijssen, J.; Herberts, C.; Drijfhout, J. W.; Reits, E.; Janssen, L.; Neefjes, J. Cross-presentation by intercellular peptide transfer through gap junctions. *Nature* **2005**, *434* (7029), 83−8.
(5) Nualart-Marti, A.; Solsona, C.; Fields, R. D. Gap junction communication in myelinating glia. *Biochim. Biophys. Acta* **2013**, *1828* (1), 69−78.
(6) Manthey, D.; Banach, K.; Desplantez, T.; Lee, C. G.; Kozak, C. A.; Traub, O.; Weingart, R.; Willecke, K. Intracellular domains of mouse connexin26 and −30 affect diffusional and electrical properties of gap junction channels. *J. Membr. Biol.* **2001**, *181* (2), 137−48.
(7) Giepmans, B. N. Role of connexin43-interacting proteins at gap junctions. *Adv. Cardiol.* **2006**, *42*, 41−56.
(8) Herve, J. C.; Derangeon, M.; Sarrouilhe, D.; Giepmans, B. N.; Bourmeyster, N. Gap junctional channels are parts of multiprotein complexes. *Biochim. Biophys. Acta* **2012**, *1818* (8), 1844−65.
(9) Elias, L. A.; Kriegstein, A. R. Gap junctions: multifaceted regulators of embryonic cortical development. *Trends Neurosci.* **2008**, *31* (5), 243−50.
(10) Elias, L. A.; Wang, D. D.; Kriegstein, A. R. Gap junction adhesion is necessary for radial migration in the neocortex. *Nature* **2007**, *448* (7156), 901−7.
(11) Miro-Casas, E.; Ruiz-Meana, M.; Agullo, E.; Stahlhofen, S.; Rodriguez-Sinovas, A.; Cabestrero, A.; Jorge, I.; Torre, I.; Vazquez, J.; Boengler, K.; Schulz, R.; Heusch, G.; Garcia-Dorado, D. Connexin43 in cardiomyocyte mitochondria contributes to mitochondrial potassium uptake. *Cardiovasc. Res.* **2009**, *83* (4), 747−56.
(12) Bergoffen, J.; Schere, S. S.; Wang, S.; Oronzi Scott, M.; Bone, L. J.; Paul, D. L.; Chen, K.; Lensch, M. W.; Chance, P. F.; Fischbeck, K. H. Connexin mutations in X-linked Charcot-Marie-Tooth disease. *Science* **1993**, *262*, 2039−42.
(13) Moennikes, O.; Buchmann, A.; Ott, T.; Willecke, K.; Schwarz, M. The effect of connexin32 null mutation on hepatocarcinogenesis in different mouse strains. *Carcinogenesis* **1999**, *20* (7), 1379−82.
(14) Krutovskikh, V.; Mazzoleni, G.; Mironov, N.; Omon, Y.; Agueloni, A.-M.; Mesnil, M.; Berger, F.; Partensky, C.; Yamasaki, H. Altered homologous and heterologous gap-junctional intercellular communicaton in primary human liver tumors associated with aberrant protein localization but not gene mutation of connexin32. *Int. J. Cancer* **1994**, *56*, 87−94.
(15) Omori, Y.; Li, Q.; Nishikawa, Y.; Yoshioka, T.; Yoshida, M.; Nishimura, T.; Enomoto, K. Pathological significance of intracytoplasmic connexin proteins: implication in tumor progression. *J. Membr. Biol.* **2007**, *218* (1−3), 73−7.
(16) Abu-Farha, M.; Lambert, J. P.; Al-Madhoun, A. S.; Elisma, F.; Skerjanc, I. S.; Figeys, D. The tale of two domains: proteomics and genomics analysis of SMYD2, a new histone methyltransferase. *Mol. Cell. Proteomics* **2008**, *7* (3), 560−72.
(17) Abu-Farha, M.; Lanouette, S.; Elisma, F.; Tremblay, V.; Butson, J.; Figeys, D.; Couture, J. F. Proteomic analyses of the SMYD family interactomes identify HSP90 as a novel target for SMYD2. *J. Mol. Cell Biol.* **2011**, *3* (5), 301−8.
(18) Ewing, R. M.; Chu, P.; Elisma, F.; Li, H.; Taylor, P.; Climie, S.; McBroom-Cerajewski, L.; Robinson, M. D.; O'Connor, L.; Li, M.; Taylor, R.; Dharsee, M.; Ho, Y.; Heilbut, A.; Moore, L.; Zhang, S.; Ornatsky, O.; Bukhman, Y. V.; Ethier, M.; Sheng, Y.; Vasilescu, J.; Abu-Farha, M.; Lambert, J. P.; Duewel, H. S.; Stewart, I. I.; Kuehl, B.; Hogue, K.; Colwill, K.; Gladwish, K.; Muskat, B.; Kinach, R.; Adams, S. L.; Moran, M. F.; Morin, G. B.; Topaloglou, T.; Figeys, D. Large-scale mapping of human protein-protein interactions by mass spectrometry. *Mol. Syst. Biol.* **2007**, *3*, 89.
(19) Nelles, E.; Buetzler, C.; Jung, D.; Temme, A.; Gabriel, H. D.; Dahl, U.; Traub, O.; Stuempel, F.; Jungermann, K.; Zielasek, J.; Toyka, K. V.; Dermietzel, R.; Willecke, K. Defective propagation of signals generated by sympathetic nerve stimulation in the liver of connexin32-deficient mice. *Proc. Natl. Acad. Sci. U.S.A.* **1996**, *93*, 9565−70.
(20) Huang da, W.; Sherman, B. T.; Lempicki, R. A. Systematic and integrative analysis of large gene lists using DAVID bioinformatics resources. *Nat. Protoc.* **2009**, *4* (1), 44−57.
(21) Fowler, S. L.; McLean, A. C.; Bennett, S. A. L. Tissue-specific cross-reactivity of connexin32 antibodies: problems and solutions unique to the central nervous system. *Cell Commun. Adhes.* **2009**, *16* (5−6), 117−30.
(22) Diez, J. A.; Ahmad, S.; Evans, W. H. Assembly of heteromeric connexons in guinea-pig liver en route to the Golgi apparatus, plasma membrane and gap junctions. *Eur. J. Biochem.* **1999**, *262* (1), 142−8.
(23) Zheng, Y. Z.; Berg, K. B.; Foster, L. J. Mitochondria do not contain lipid rafts, and lipid rafts do not contain mitochondrial proteins. *J. Lipid Res.* **2009**, *50* (5), 988−98.
(24) Naz, N.; Moriconi, F.; Ahmad, S.; Amanzada, A.; Khan, S.; Mihm, S.; Ramadori, G.; Malik, I. A. Ferritin L is the sole serum ferritin constituent and a positive hepatic acute phase protein. *Shock* **2013**.
(25) Palatinus, J. A.; Rhett, J. M.; Gourdie, R. G. The connexin43 carboxyl terminus and cardiac gap junction organization. *Biochim. Biophys. Acta* **2012**, *1818* (8), 1831−43.
(26) Singh, D.; Lampe, P. D. Identification of connexin-43 interacting proteins. *Cell Commun. Adhes.* **2003**, *10* (4−6), 215−20.
(27) Singh, D.; Solan, J. L.; Taffet, S. M.; Javier, R.; Lampe, P. D. Connexin 43 interacts with zona occludens-1 and −2 proteins in a cell cycle stage-specific manner. *J. Biol. Chem.* **2005**, *280* (34), 30416−21.
(28) Zhou, H.; Wang, F.; Wang, Y.; Ning, Z.; Hou, W.; Wright, T. G.; Sundaram, M.; Zhong, S.; Yao, Z.; Figeys, D. Improved recovery and identification of membrane proteins from rat hepatic cells using a centrifugal proteomic reactor. *Mol. Cell. Proteomics* **2011**, *10* (10), O111 008425.
(29) Locke, D.; Harris, A. L. Connexin channels and phospholipids: association and modulation. *BMC Biol.* **2009**, *7*, 52.
(30) Kojima, T.; Kokai, Y.; Chiba, H.; Yamamoto, M.; Mochizuki, Y.; Sawada, N. Cx32 but not Cx26 is associated with tight junctions in primary cultures of rat hepatocytes. *Exp. Cell Res.* **2001**, *263* (2), 193−201.
(31) Penes, M. C.; Li, X.; Nagy, J. I. Expression of zonula occludens-1 (ZO-1) and the transcription factor ZO-1-associated nucleic acid-binding protein (ZONAB)-MsY3 in glial cells and colocalization at oligodendrocyte and astrocyte gap junctions in mouse brain. *Eur. J. Neurosci.* **2005**, *22* (2), 404−18.
(32) Schubert, A. L.; Schubert, W.; Spray, D. C.; Lisanti, M. P. Connexin family members target to lipid raft domains and interact with caveolin-1. *Biochemistry* **2002**, *41* (18), 5754−64.
(33) Torok, K.; Stauffer, K.; Evans, W. H. Connexin 32 of gap junctions contains two cytoplasmic calmodulin-binding domains. *Biochem. J.* **1997**, *326* (Pt2), 479−83.
(34) Duffy, H. S.; Iacobas, I.; Hotchkiss, K.; Hirst-Jensen, B. J.; Bosco, A.; Dandachi, N.; Dermietzel, R.; Sorgen, P. L.; Spray, D. C. The gap junction protein connexin32 interacts with the Src homology

3/hook domain of discs large homolog 1. *J. Biol. Chem.* **2007**, *282* (13), 9789−96.
(35) Delmar, M. Gap junction gating and its molecular control. In *International Gap Junction Conference 2011*; Ghent University: Belgium, 2011; p 30.
(36) Sato, P. Y.; Coombs, W.; Lin, X.; Nekrasova, O.; Green, K. J.; Isom, L. L.; Taffet, S. M.; Delmar, M. Interactions between ankyrin-G, Plakophilin-2, and Connexin43 at the cardiac intercalated disc. *Circ. Res.* **2011**, *109* (2), 193−201.
(37) Boengler, K.; Stahlhofen, S.; van de Sand, A.; Gres, P.; Ruiz-Meana, M.; Garcia-Dorado, D.; Heusch, G.; Schulz, R. Presence of connexin 43 in subsarcolemmal, but not in interfibrillar cardiomyocyte mitochondria. *Basic Res. Cardiol.* **2009**, *104* (2), 141−7.
(38) Rottlaender, D.; Boengler, K.; Wolny, M.; Michels, G.; Endres-Becker, J.; Motloch, L. J.; Schwaiger, A.; Buechert, A.; Schulz, R.; Heusch, G.; Hoppe, U. C. Connexin 43 acts as a cytoprotective mediator of signal transduction by stimulating mitochondrial KATP channels in mouse cardiomyocytes. *J. Clin. Invest.* **2010**, *120* (5), 1441−53.
(39) Rottlaender, D.; Boengler, K.; Wolny, M.; Schwaiger, A.; Motloch, L. J.; Ovize, M.; Schulz, R.; Heusch, G.; Hoppe, U. C. Glycogen synthase kinase 3beta transfers cytoprotective signaling through connexin 43 onto mitochondrial ATP-sensitive K+ channels. *Proc. Natl. Acad. Sci. U.S.A.* **2012**, *109* (5), E242−51.
(40) Ruiz-Meana, M.; Rodriguez-Sinovas, A.; Cabestrero, A.; Boengler, K.; Heusch, G.; Garcia-Dorado, D. Mitochondrial connexin43 as a new player in the pathophysiology of myocardial ischaemia-reperfusion injury. *Cardiovasc. Res.* **2008**, *77* (2), 325−33.
(41) Lebiedzinska, M.; Szabadkai, G.; Jones, A. W.; Duszynski, J.; Wieckowski, M. R. Interactions between the endoplasmic reticulum, mitochondria, plasma membrane and other subcellular organelles. *Int. J. Biochem. Cell Biol.* **2009**, *41* (10), 1805−16.
(42) Li, X.; Han, D.; Kin Ting Kam, R.; Guo, X.; Chen, M.; Yang, Y.; Zhao, H.; Chen, Y. Developmental expression of sideroflexin family genes in Xenopus embryos. *Dev. Dyn.* **2010**, *239* (10), 2742−7.
(43) Miotto, G.; Tessaro, S.; Rotta, G. A.; Bonatto, D. In silico analyses of Fsf1 sequences, a new group of fungal proteins orthologous to the metazoan sideroblastic anemia-related sideroflexin family. *Fungal Genet. Biol.* **2007**, *44* (8), 740−53.
(44) Ye, X.; Xu, J.; Cheng, C.; Yin, G.; Zeng, L.; Ji, C.; Gu, S.; Xie, Y.; Mao, Y. Isolation and characterization of a novel human putative anemia-related gene homologous to mouse sideroflexin. *Biochem Genet* **2003**, *41* (3−4), 119−25.
(45) Fleming, M. D.; Campagna, D. R.; Haslett, J. N.; Trenor, C. C., , 3rd; Andrews, N. C. A mutation in a mitochondrial transmembrane protein is responsible for the pleiotropic hematological and skeletal phenotype of flexed-tail (f/f) mice. *Genes Dev.* **2001**, *15* (6), 652−7.
(46) Berthoud, V. M.; Iwanij, V.; Garcia, A. M.; Saez, J. C. Connexins and glucagon receptors during development of rat hepatic acinus. *Am. J. Physiol.* **1992**, *263* (5 Pt 1), G650−8.
(47) Bilello, J. P.; Cable, E. E.; Isom, H. C. Expression of E-cadherin and other paracellular junction genes is decreased in iron-loaded hepatocytes. *Am. J. Pathol.* **2003**, *162* (4), 1323−38.
(48) Beaton, M. D.; Adams, P. C. Treatment of hyperferritinemia. *Ann. Hepatol.* **2012**, *11* (3), 294−300.
(49) Krutovskikh, V.; Mesnil, M.; Mazzoleni, G.; Yamasaki, H. Inhibition of rat liver gap junction intercellular communication by tumor-promoting agents in vivo. Association with aberrant localization of connexin proteins. *Lab. Invest.* **1995**, *72*, 571−7.
(50) Liu, C. L.; Huang, Y. S.; Hosokawa, M.; Miyashita, K.; Hu, M. L. Inhibition of proliferation of a hepatoma cell line by fucoxanthin in relation to cell cycle arrest and enhanced gap junctional intercellular communication. *Chem. Biol. Interact.* **2009**, *182* (2−3), 165−72.
(51) Mizuarai, S.; Miki, S.; Araki, H.; Takahashi, K.; Kotani, H. Identification of dicarboxylate carrier Slc25a10 as malate transporter in de novo fatty acid synthesis. *J. Biol. Chem.* **2005**, *280* (37), 32434−41.
(52) Leung, T. M.; Lu, Y.; Yan, W.; Moron-Concepcion, J. A.; Ward, S. C.; Ge, X.; Conde de la Rosa, L.; Nieto, N. Argininosuccinate synthase conditions the response to acute and chronic ethanol-induced liver injury in mice. *Hepatology* **2012**, *55* (5), 1596−609.
(53) Lee, C. F.; Ling, Z. Q.; Zhao, T.; Fang, S. H.; Chang, W. C.; Lee, S. C.; Lee, K. R. Genomic-wide analysis of lymphatic metastasis-associated genes in human hepatocellular carcinoma. *World J. Gastroenterol.* **2009**, *15* (3), 356−65.
(54) Faghfoury, H.; Baruteau, J.; de Baulny, H. O.; Haberle, J.; Schulze, A. Transient fulminant liver failure as an initial presentation in citrullinemia type I. *Mol. Genet. Metab.* **2011**, *102* (4), 413−7.
(55) Detke, S.; Elsabrouty, R. Leishmania mexicana amazonensis: plasma membrane adenine nucleotide translocator and chemotaxis. *Exp. Parasitol.* **2008**, *118* (3), 408−19.
(56) Loers, G.; Makhina, T.; Bork, U.; Dorner, A.; Schachner, M.; Kleene, R. The interaction between cell adhesion molecule L1, matrix metalloproteinase 14, and adenine nucleotide translocator at the plasma membrane regulates L1-mediated neurite outgrowth of murine cerebellar neurons. *J. Neurosci.* **2012**, *32* (11), 3917−30.
(57) Radichev, I. A.; Remacle, A. G.; Sounni, N. E.; Shiryaev, S. A.; Rozanov, D. V.; Zhu, W.; Golubkova, N. V.; Postnova, T. I.; Golubkov, V. S.; Strongin, A. Y. Biochemical evidence of the interactions of membrane type-1 matrix metalloproteinase (MT1-MMP) with adenine nucleotide translocator (ANT): potential implications linking proteolysis with energy metabolism in cancer cells. *Biochem. J.* **2009**, *420* (1), 37−47.
(58) Sigal, C. T.; Resh, M. D. The ADP/ATP carrier is the 32-kilodalton receptor for an NH2-terminally myristylated src peptide but not for pp60src polypeptide. *Mol. Cell. Biol.* **1993**, *13* (5), 3084−92.
(59) Woudenberg, J.; Rembacz, K. P.; van den Heuvel, F. A.; Woudenberg-Vrenken, T. E.; Buist-Homan, M.; Geuken, M.; Hoekstra, M.; Deelman, L. E.; Enrich, C.; Henning, R. H.; Moshage, H.; Faber, K. N. Caveolin-1 is enriched in the peroxisomal membrane of rat hepatocytes. *Hepatology* **2010**, *51* (5), 1744−53.
(60) Fort, A. G.; Murray, J. W.; Dandachi, N.; Davidson, M. W.; Dermietzel, R.; Wolkoff, A. W.; Spray, D. C. In vitro motility of liver connexin vesicles along microtubules utilizes kinesin motors. *J. Biol. Chem.* **2011**, *286* (26), 22875−85.
(61) Garcia, J. The calcium channel alpha2/delta1 subunit interacts with ATP5b in the plasma membrane of developing muscle cells. *Am. J. Physiol. Cell Physiol.* **2011**, *301* (1), C44−52.